Supporting Information

Towards Catalytic Fluoroquinolones: From Metal-Catalyzed to Metal-Free DNA Cleavage

Moshe N. Goldmeier[a,†], Alina Khononov[a,†], Tomasz Pieńko[a,†], Valery Belakhov[a], Feng-Chun Yen[b], Limor Baruch [b], Marcelle Machluf [b], and Timor Baasov[a,*]

[a] Edith and Joseph Fischer Enzyme Inhibitors Laboratory, Schulich Faculty of Chemistry, Technion – Israel Institute of Technology, Haifa 3200003, Israel.

[b] Faculty of Biotechnology and Food Engineering, Technion – Israel Institute of Technology, Haifa 3200003, Israel.

[†] Equal contribution, [*]Corresponding author e-mail: chtimor@technion.ac.il

Contents

I. Experimental Section

1. Supplementary figures for DNase assays

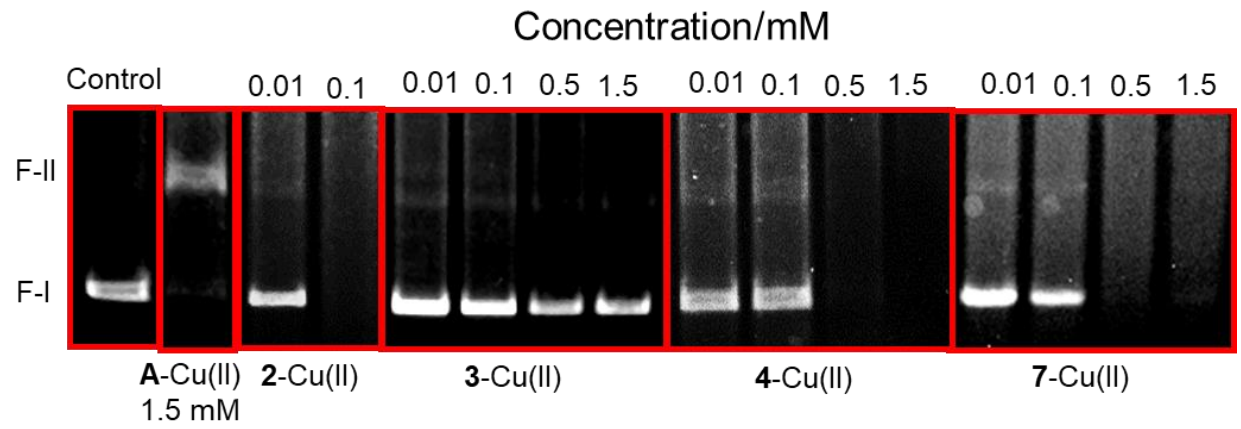

Figure S1. DNase assay for **2**-Cu(II), **3**-Cu(II), **4**-Cu(II) and **7**-Cu(II) compounds. Comparative concentration dependent cleavage of (+) supercoiled pHOT-1 plasmid (0.014 μg μL^{-1}) in HEPES buffer (50 mM, pH 7.4) over 5 h. Compounds include **A**-Cu(II) as positive control.

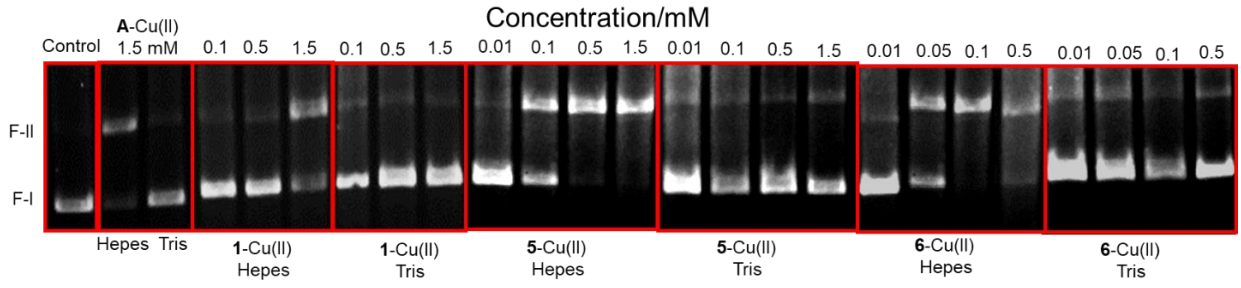

Figure S2. DNase assay for **15**-Cu(II), **19**-Cu(II) and **20-Cu(II)** complexes. Comparative concentration dependent cleavage of (+) supercoiled pHOT-1 plasmid (0.014 μg μL^{-1}) in HEPES buffer (50 mM, pH 7.4) and Tris-HCl (50 mM, pH 7.4) buffer over 5 h. Compounds include **A**-Cu(II) as positive control.

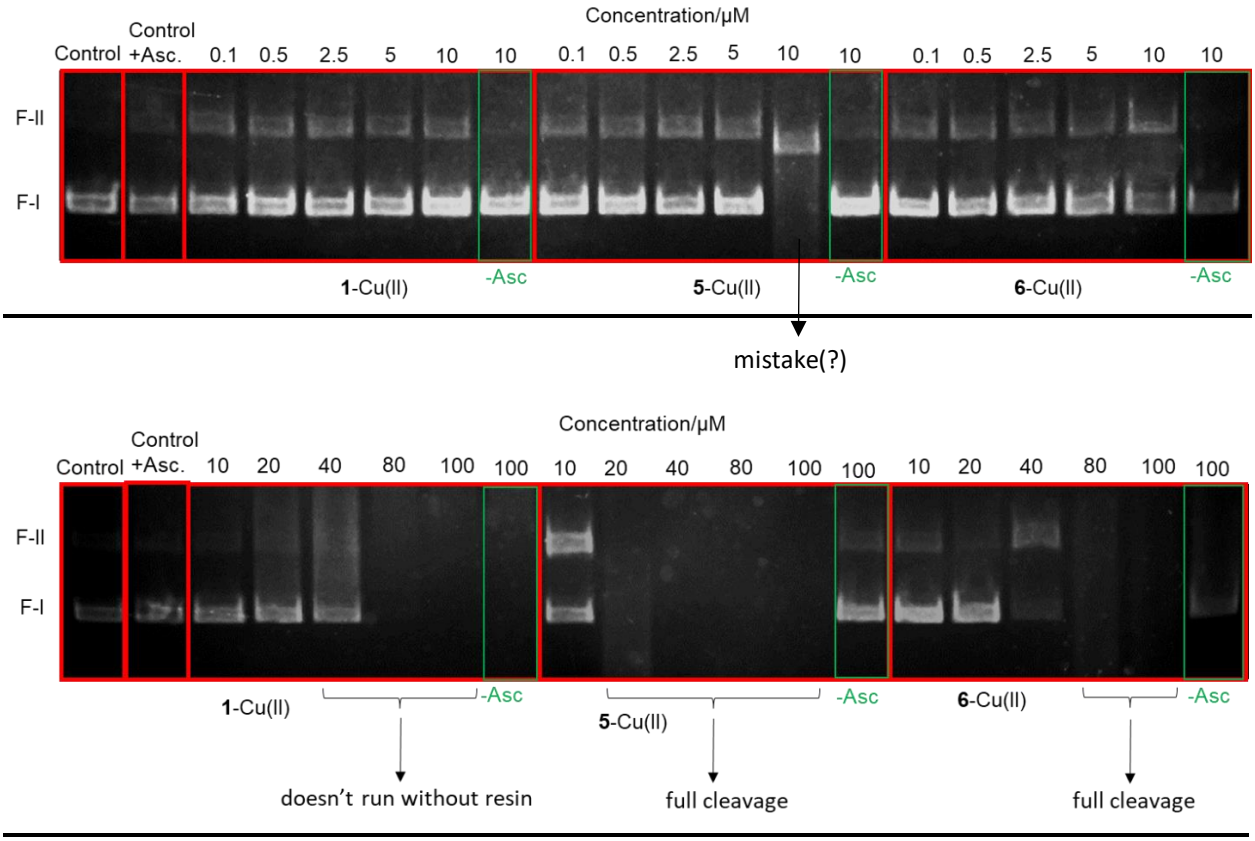

Figure S3. DNase assay in the presence of ascorbic acid (0.32 mM) for Cu(II) complexes of **1**, **5** and **6** at the concentrations of 0.1-10 μM (top panel) and at 10-100 μM (bottom panel). Comparative concentration dependent cleavage of (+) supercoiled pHOT-1 plasmid (0.014 μg μL^{-1}) in HEPES buffer (50 mM, pH 7.4) and ascorbic acid (0.32 mM) over 2 h.

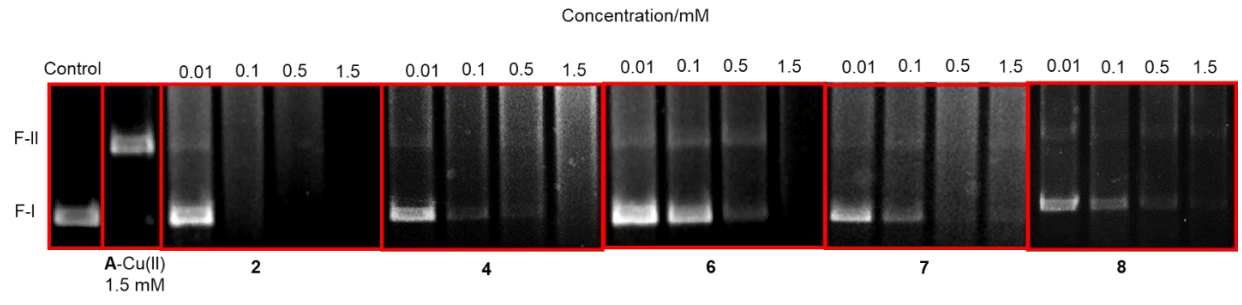

Figure S4. DNase assay for compounds **2**, **4**, and **6-8**. Comparative concentration dependent cleavage of (+) supercoiled pHOT-1 plasmid (0.014 μg μL^{-1}) in HEPES buffer (50 mM, pH 7.4) over 5 h. Compounds include **A**-Cu(II) as positive control.

2. Analytical data for compounds **13b-d** and **14a-d**

Compound 13b.

Steps 1-2. Following the general procedure, compounds **11b** (1.44 g, 2.65 mmol) and **12** (1.76 g, 3.31 mmol) yielded 48% of the corresponding phthalimide derivative (1.1 g, 1.27 mmol); ^{1}H NMR (600 MHz, $CDCl_3$) δ_H 8.48 (s, 1H, QH-2), 7.98 (d, 1H, QH-5), 7.78-7.76 (m, 2H, phthalimide Ar), 7.65-7.63 (m, 2H, phthalimide Ar), 7.21-7.17 (m, 3H, QH-8, linker Ar), 7.06 (d, 2H, linker Ar), 3.86 (s, 3H, OCH_3), 3.69-3.67 (m, 2H, phthalimide), 3.50 (bs, 2H, Ph-C$\underline{H_2}$-piperazine), 3.36-3.35 (m, 1H, cyclopropane CH), 3.22-3.18 (m, 8H, piperazine (4H), TACN (4H)), 2.83-2.76 (m, 6H, TACN (4H), phtalimide (2H)), 2.65-2.54 (m, 12H, piperazine (4H), TACN (4H)), TACN-CH_2C$\underline{H_2}$-Ph (2H), TACN-C$\underline{H_2}C H_2$-Ph (2H)), 1.40-1.38 (m, 9H, Boc), 1.25-1.23 (d, 2H, cyclopropane CH_2), 1.08-1.05 (m, 2H, cyclopropane CH_2); ^{13}C NMR (150 MHz, $CDCl_3$) δ_C 174.26 (cipro C=O), 166.52 (phthalimide C=O), 165.42 (cipro C=O), 158.63 (Boc C=O), 158.42 (cipro), 149.66 (cipro), 147.87, 145.64 (cipro), 142.37 (linker Ar), 140.05, 136.54 (cipro), 134.58 (linker Ar), 133.86, 132.85 (C-H phthalimide Ar), 132.54 (phthalimide Ar), 129.45, 127.22 (C-H linker Ar), 126.74 (C-H linker Ar), 124.34 (C-H phthalimide Ar), 123.11 (cipro), 110.45 (cipro), 107.76 (cipro), 106.65, 103.87 (cipro), 78.87 (Boc $\underline{C}(CH_3)_3$), 64.45 (Ph-$\underline{C}H_2$-piperazine), 59.23, 55.68, 53.10 ($\underline{C}H_2$N), 51.54 (piperazine), 51.76 (O$\underline{C}H_3$), 49.78 (piperazine), 48.65 ($\underline{C}H_2$N), 38.01 ($\underline{C}H_2$-phthalimide), 33.98 (cyclopropane $\underline{C}$H), 31.59 (TACN-$CH_2\underline{C}H_2$-Ph), 27.48 (TACN-$\underline{C}H_2CH_2$-Ph), 25.52 (Boc C($\underline{C}H_3)_3$), 7.98 (cyclopropane $\underline{C}H_2$). MS (ESI+ QTOFMS) calculated for $C_{48}H_{59}FN_7O_7$ ($[M+H]^+$) *m/z* 864.44; measured *m/z* 864.45.

Step 3. Following the general procedure, the phthalimide derivative (1.35 g, 1.57 mmol) yielded 74% of compound **13b** (0.85 g, 1.16 mmol); ^{1}H NMR (600 MHz, $CDCl_3$) δ_H 9.83 (m, 1H, CH_3-N$\underline{H}$-CO), 8.75 (s, 1H, QH-2), 7.96-7.93 (d, 1H, QH-5), 7.26-7.13 (m, 5H, QH-8 (1H), linker Ar (4H)), 3.50-3.48 (m, 2H, Ph-C$\underline{H_2}$-piperazine), 3.40-3.39 (m, 2H, cyclopropane CH (1H), CH_2N (1H)), 3.24-3.18 (m, 8H, CH_2N(4H), piperazine (4H)), 2.93-2.91 (m, 6H, C$\underline{H_3}$-NH-CO (3H), CH_2N (3H)), 2.90-2.87 (m, 3H, CH_2N), 2.86-2.82 (m, 4H, piperazine), 2.76-2.72 (m, 7H, TACN-C$\underline{H_2}CH_2$-Ph (2H), TACN-CH_2C$\underline{H_2}$-Ph (2H), CH_2N (3H)), 2.71, 2.41 (m, 1H, CH_2N), 1.40-1.34 (s, 9H, Boc), 1.26-1.21 (m, 2H, cyclopropane CH_2), 1.09-1.07 (m, 2H, cyclopropane CH_2); ^{13}C NMR (150 MHz, $CDCl_3$) δ_C 175.49 (cipro C=O), 165.65 (cipro C=O), 156.48, 154.26 (Boc C=O), 152.61 (cipro), 146.55 (cipro C-H), 145.03 (cipro), 138.48 (linker Ar), 135.50 (cipro), 129.36 (C-H linker Ar), 128.81 (C-H linker Ar), 121.73 (cipro), 112.44 (cipro C-H), 111.36 (cipro), 104.71 (cipro C-H), 80.14 (Boc $\underline{C}(CH_3)_3$), 62.65 (Ph-$\underline{C}H_2$-piperazine), 52.74 (piperazine), 50.01 ($\underline{C}H_2$N), 45.81 (piperazine), 39.27 ($\underline{C}H_2$-NH_2), 34.66 (cyclopropane $\underline{C}$H), 28.64 (Boc C($\underline{C}H_3)_3$), 25.86 ($\underline{C}H_3$-NH-CO), 9.47, 8.21 (cyclopropane $\underline{C}H_2$). MS (ESI+ QTOFMS) calculated for $C_{40}H_{58}FN_8O_4$ ($[M+H]^+$) *m/z* 733.42; measured *m/z* 733.39.

Compound 13c.

Steps 1-2. Following the general procedure, compounds **11c** (1.6 g, 2.88 mmol) and **12** (1.91 g, 3.6 mmol) yielded 41% of the corresponding phthalimide derivative (1.036 g, 1.18 mmol); ^{1}H NMR (600 MHz, $CDCl_3$) δ_H 8.52 (s, 1H, QH-2), 7.99 (d, 1H, QH-5), 7.86-7.79 (m, 2H, phthalimide Ar), 7.74-7.67 (m, 2H, phthalimide Ar), 7.27-7.23 (m, 3H, QH-8, linker Ar), 7.13 (d, 2H, linker Ar), 3.91 (s, 3H, OCH_3), 3.79-3.72 (m, 2H, phthalimide), 3.56 (bs, 2H, Ph-C$\underline{H_2}$-piperazine), 3.44-3.39 (m, 1H, cyclopropane CH), 3.38-3.32 (m, 2H, TACN), 3.31-3.21 (m, 6H, piperazine (4H), TACN (2H)), 3.03-2.97 (m, 1H, TACN), 2.97-2.92 (m, 1H, TACN), 2.89-2.81 (m, 2H, phthalimide), 2.80-2.61 (m, 8H, piperazine (4H), TACN (4H)), 2.60-2.52 (m, 4H, TACN-$(CH_2)_2$C$\underline{H_2}$-Ph (2H), TACN (2H)), 2.52-2.44 (m, 2H, TACN-C$\underline{H_2}(CH_2)_2$-Ph), 1.78-1.60 (m, 2H, TACN-CH_2C$\underline{H_2}CH_2$-Ph), 1.44, 1.43 (s, 9H, Boc), 1.33-1.27 (m, 2H, cyclopropane CH_2), 1.15-1.10 (m, 2H, cyclopropane CH_2); ^{13}C NMR (150 MHz, $CDCl_3$) δ_C 173.06 (cipro C=O), 168.39 (phthalimide C=O), 166.47 (cipro C=O), 155.43 (Boc C=O), 153.43 (cipro), 148.32 (cipro), 144.72 (cipro), 141.42, 141.32 (linker Ar), 138.00 (cipro), 135.05 (linker Ar), 133.96, 133.89 (C-H phthalimide Ar), 132.17, 132.13 (phthalimide Ar), 129.24 (C-H linker Ar), 128.35, 128.32 (C-H linker Ar), 123.16, 123.14 (C-H phthalimide Ar), 122.89 (cipro), 113.20 (cipro), 109.99 (cipro), 104.75 (cipro), 79.17 (Boc $\underline{C}(CH_3)_3$), 62.72 (Ph-$\underline{C}H_2$-piperazine), 57.81, 57.58, 55.14, 54.38, 54.11 ($\underline{C}H_2N$), 52.78 (piperazine), 52.04 (O$\underline{C}H_3$), 50.00 (piperazine), 49.53 ($\underline{C}H_2N$), 36.38, 36.22 ($\underline{C}H_2$-phthalimide), 34.50 (cyclopropane $\underline{C}H$), 33.35, 33.24 (TACN-$(CH_2)_2\underline{C}H_2$-Ph), 28.63-28.50 (TACN-$CH_2\underline{C}H_2CH_2$-Ph, Boc C($\underline{C}H_3)_3$), 8.12 (cyclopropane $\underline{C}H_2$). MS (ESI+ QTOFMS) calculated for $C_{49}H_{61}FN_7O_7$ ($[M+H]^+$) *m/z* 878.46; measured *m/z* 878.41.

Step 3. Following the general procedure, the phthalimide derivative (1.37 g, 1.56 mmol) yielded 70% of compound **13c** (0.815 g, 1.09 mmol);
^{1}H NMR (600 MHz, $CDCl_3$) δ_H 9.95-9.84 (m, 1H, CH_3-N$\underline{H}$-CO), 8.82 (s, 1H, QH-2), 8.01 (d, 1H, QH-5), 7.32 (d, 1H, QH-8), 7.27 (d, 2H, linker Ar), 7.19 (d, 2H, linker Ar), 3.60-3.55 (m, 2H, Ph-C$\underline{H_2}$-piperazine), 3.52-3.43 (m, 2H, cyclopropane CH (1H), CH_2N (1H)), 3.41-3.33 (m, 3H, CH_2N), 3.33-3.23 (m, 5H, piperazine (4H), CH_2N (1H)), 3.02-2.97 (m, 4H, C$\underline{H_3}$-NH-CO (3H), CH_2N (1H)), 2.91-2.75 (m, 6H, CH_2N), 2.71-2.66 (m, 4H, piperazine), 2.65-2.54 (m, 7H, TACN-C$\underline{H_2}(CH_2)_2$-Ph (2H), TACN-$(CH_2)_2$C$\underline{H_2}$-Ph (2H), CH_2N (3H)), 2.53-2.49 (m, 1H, CH_2N), 1.85-1.73 (m, 2H, TACN-CH_2C$\underline{H_2}CH_2$-Ph), 1.47, 1.46 (s, 9H, Boc), 1.34-1.30 (m, 2H, cyclopropane CH_2), 1.18-1.14 (m, 2H, cyclopropane CH_2); ^{13}C NMR (150 MHz, $CDCl_3$) δ_C 175.48 (cipro C=O), 165.63 (cipro C=O), 156.12, 155.40 (Boc C=O), 153.44 (cipro), 146.53 (cipro C-H), 144.98 (cipro), 141.16 (linker Ar), 138.47 (cipro), 135.14, 135.08 (linker Ar), 129.31 (C-H linker Ar), 128.35 (C-H linker Ar), 121.72 (cipro), 112.53 (cipro C-H), 111.37 (cipro), 104.67 (cipro C-H), 79.74, 79.45 (Boc $\underline{C}(CH_3)_3$), 62.71 (Ph-$\underline{C}H_2$-piperazine), 58.31, 58.07, 55.76, 55.39, 54.91, 54.58, 54.40, 53.91 ($\underline{C}H_2N$), 52.76 (piperazine), 52.04, 51.71, 51.50, 50.95 ($\underline{C}H_2N$), 50.03 (piperazine), 39.38, 39.24 ($\underline{C}H_2$-NH_2), 34.64 (cyclopropane $\underline{C}H$), 33.48, 33.38 (TACN-$(CH_2)_2\underline{C}H_2$-Ph), 28.67-28.49 (TACN-$CH_2\underline{C}H_2CH_2$-Ph, Boc C($\underline{C}H_3)_3$), 25.84 ($\underline{C}H_3$-NH-CO), 8.19 (cyclopropane $\underline{C}H_2$). MS (ESI+ QTOFMS) calculated for $C_{41}H_{60}FN_8O_4$ ($[M+H]^+$) *m/z* 747.47; measured *m/z* 747.40.

Compound 13d.

Steps 1-2. Following the general procedure, compounds **11d** (1.53 g, 2.69 mmol) and **12** (1.78 g, 3.36 mmol) yielded 51% of the corresponding phthalimide derivative (1.217 g, 1.37 mmol); ^{1}H NMR (600 MHz, $CDCl_3$) δ_H 8.47 (s, 1H, QH-2), 7.93 (d, 1H, QH-5), 7.79-7.76 (m, 1H, phthalimide Ar), 7.68-7.66 (m, 2H, phthalimide Ar), 7.38-7.34 (m, 1H, phthalimide Ar), 7.21-7.18 (m, 3H, QH-8, linker Ar), 7.07-7.05 (m, 1H, linker Ar), 6.98 (d, 1H, linker Ar), 3.83 (s, 3H, OCH_3), 3.71, 3.64, 3.52-3.47 (m, 5H, phthalimide (2H), Ph-C*H*$_2$-piperazine (2H), cyclopropane CH (1H)), 3.36-3.34 (m, 2H, TACN), 3.25-3.17 (m, 6H, piperazine (4H), TACN (2H)), 3.07-3.04 (m, 4H, TACN(2H), phthalimide(2H)), 2.89-2.86 (m, 8H, piperazine (4H), TACN (4H)), 2.61-2.56 (m, 4H, TACN-$(CH_2)_3$C*H*$_2$-Ph (2H), TACN (2H)), 2.38-2.31 (m, 2H, TACN-C*H*$_2$$(CH_2)_3$-Ph), 1.40-1.38 (m, 4H, TACN-CH_2(C*H*$_2$$)_2CH_2$-Ph), 1.29-1.27 (m, 9H, Boc), 1.24-1.23 (m, 2H, cyclopropane CH_2), 1.05 (m, 2H, cyclopropane CH_2); ^{13}C NMR (150 MHz, $CDCl_3$) δ_C 172.89 (cipro C=O), 167.54 (phthalimide C=O), 168.52 (cipro C=O), 156.01 (Boc C=O), 155.81 (cipro), 149.82 (cipro), 145.98, 140.85 (cipro), 139.62 (linker Ar), 137.86 (cipro), 136.01, 134.99 (linker Ar), 134.02 (C-H phthalimide Ar), 132.95, 130.84 (phthalimide Ar), 128.14 (C-H linker Ar), 126.28 (C-H linker Ar), 124.64 (C-H phthalimide Ar), 123.01 (cipro), 118.99, 114.15 (cipro), 110.28 (cipro), 102.88 (cipro), 77.67 (Boc *C*$(CH_3)_3$), 64.00 (Ph-*C*H_2-piperazine), 59.16, 56.16 (*C*H_2N), 54.53 (piperazine), 51.87 (O*C*H_3), 50.52 (piperazine), 49.54, 48.07 (*C*H_2N), 38.27 (*C*H_2-phthalimide), 35.40 (cyclopropane *C*H), 33.35 (TACN-*C*$H_2$$(CH_2)_2CH_2$-Ph), 30.26 (TACN-$(CH_2)_3$*C*$H_2$-Ph), 29.75-28.70 (TACN-$CH_2$(*C*$H_2$$)_2CH_2$-Ph, Boc C(*C*$H_3$$)_3$), 8.06 (cyclopropane *C*H_2). MS (ESI+ QTOFMS) calculated for $C_{49}H_{61}FN_7O_7$ ($[M+H]^+$) *m/z* 892.49; measured *m/z* 892.58.

Step 3. Following the general procedure, the phthalimide derivative (1.22 g, 1.37 mmol) yielded 79% of compound **13d** (0.82 g, 1.08 mmol);

^{1}H NMR (600 MHz, $CDCl_3$) δ_H 9.83 (m, 1H, CH_3-N*H*-CO), 8.75 (s, 1H, QH-2), 7.96 (d, 1H, QH-5), 7.37 (d, 1H, QH-8), 7.27-7.25 (d, 2H, linker Ar), 7.10 (d, 2H, linker Ar), 3.51 (m, 2H, Ph-C*H*$_2$-piperazine), 3.40-3.38 (m, 2H, cyclopropane CH (1H), CH_2N (1H)), 3.29-3.24 (m, 9H, piperazine (4H), CH_2N (5H)), 3.13 (m, 3H, C*H*$_3$-NH-CO), 2.93-2.87 (m, 6H, CH_2N), 2.73-2.51 (m, 12H, piperazine (4H), TACN-C*H*$_2$$(CH_2)_3$-Ph (2H), TACN-$(CH_2)_3$C*H*$_2$-Ph (2H), CH_2N (4H)), 2.37-2.30 (m, 4H, TACN-CH_2(C*H*$_2$$)_2CH_2$-Ph), 1.57, 1.43-1.38 (m, 9H, Boc), 1.26-1.24 (m, 2H, cyclopropane CH_2), 1.10-1.07 (m, 2H, cyclopropane CH_2); ^{13}C NMR (150 MHz, $CDCl_3$) δ_C 176.02 (cipro C=O), 167.83 (cipro C=O), 156.40 (Boc C=O), 155.86, 154.08 (cipro), 148.45 (cipro C-H), 145.97 (cipro), 140.46 (linker Ar), 138.57, 137.45 (cipro), 134.58 (linker Ar), 132.87, 130.52 (C-H linker Ar), 129.07 (C-H linker Ar), 123.68 (cipro), 116.23, 111.53 (cipro C-H), 109.52 (cipro), 105.74 (cipro C-H), 80.01 (Boc *C*$(CH_3)_3$), 76.54, 64.73 (Ph-*C*H_2-piperazine), 58.76, 57.82, 55.91, 52.54 (*C*H_2N), 52.34 (piperazine), 50.49, 48.67 (*C*H_2N), 48.12, 47.73 (piperazine), 41.54 (*C*H_2-NH_2), 33.78 (cyclopropane *C*H), 32.24 (TACN-$(CH_2)_3$*C*H_2-Ph), 29.69-26.54 (TACN-CH_2(*C*$H_2$$)_2CH_2$-Ph, Boc C(*C*$H_3$$)_3$), 26.74 (*C*$H_3$-NH-CO), 7.98 (cyclopropane *C*H_2). MS (ESI+ QTOFMS) calculated for $C_{42}H_{62}FN_8O_4$ ($[M+H]^+$) *m/z* 761.48; measured *m/z* 761.63.

Compound 14a

Following the general procedure, compounds **13a** (0.748 g, 1.04 mmol) and N,N-di-Boc-1H-pyrazole-1-carboxamidine (0.323 g, 1.04 mmol) yielded 72% of compound **14a** (0.72 g, 0.75 mmol);

^{1}H NMR (600 MHz, $CDCl_3$) δ_H 11.44 (d, 1H, Boc-N*H*-guanidine), 9.84 (q, 1H, CH_3-N*H*-CO), 8.76 (s, 1H, QH-2), 8.66-8.65 (m, 1H, guanidine N*H*), 7.96 (d, 1H, QH-5), 7.26-.21 (m, 5H, QH-8 (1H), linker Ar (4H)), 3.64 (s, 2H, Ph-C*H*$_2$-piperazine), 3.42-3.36 (m, 7H, C*H*$_2$-guanidine (2H), cyclopropane CH (1H), CH_2N (4H)), 3.24 (m, 4H, piperazine), 2.93 (d, 3H, C*H*$_3$-NH-CO), 2.93-2.92 (m, 2H, CH_2N), 2.89-2.84 (m, 1H, CH_2N), 2.71-2.62 (m, 9H, piperazine (4H), CH_2N (3H), TACN-C*H*$_2$-Ph (2H)), 1.44-1.39 (m, 27H, Boc), 1.26-1.25 (m, 2H, cyclopropane CH_2), 1.09-1.08 (m, 2H, cyclopropane CH_2); ^{13}C NMR (150 MHz, $CDCl_3$) δ_C 175.50 (cipro C=O), 165.66 (cipro C=O), 163.58 (guanidine C), 156.11, 156.06 (Boc C=O), 155.50, 155.42 (Boc C=O), 154.28 (cipro), 153.00 (Boc C=O), 152.63, 146.55 (cipro C-H), 145.07 (cipro), 138.47 (cipro), 129.11 (C-H linker Ar), 128.85 (linker Ar), 121.76 (cipro), 111.35 (cipro C-H), 104.67 (cipro C-H), 79.28 (Boc *C*$(CH_3)_3$), 62.69 (s, Ph-*C*H_2-piperazine), 57.27, 52.77 (s, piperazine), 49.99 (s, *C*H_2N), 49.84 (piperazine), 48.65 (*C*H_2N), 39.26 (*C*H_2-guanidine), 34.65 (cyclopropane *C*H), 29.71 (s, TACN-*C*H_2-Ph), 28.60 (Boc C(*C*$H_3)_3$), 28.31 (Boc C(*C*$H_3)_3$), 28.07 (Boc C(*C*$H_3)_3$), 25.87 (*C*H_3-NH-CO), 8.20 (cyclopropane *C*H_2). MS (ESI+ QTOFMS) calculated for $C_{50}H_{74}FN_{10}O_8$ ($[M+H]^+$) *m/z* 961.56; measured *m/z* 961.56.

Compound 14b

Following the general procedure, compounds **13b** (0.654 g, 0.893 mmol) and N,N-di-Boc-1H-pyrazole-1-carboxamidine (0.277 g, 0.893 mmol) yielded 75% of compound **14b** (0.654 g, 0.67 mmol);

^{1}H NMR (600 MHz, $CDCl_3$) δ_H 11.43 (d, 1H, Boc-N*H*-guanidine), 9.83 (q, 1H, CH_3-N*H*-CO), 8.76 (s, 1H, QH-2), 7.97-7.95 (m, 1H, guanidine N*H*), 7.66-7.65 (m, 2H, QH-5, QH-8), 7.49-7.47 (m, 2H, linker Ar), 7.27.12 (m, 2H, linker Ar), 3.52 (s, 2H, Ph-C*H*$_2$-piperazine), 3.39-3.27 (m, 7H, C*H*$_2$-guanidine (2H), cyclopropane CH (1H), CH_2N (4H)), 3.25-3.18 (m, 4H, piperazine), 2.94 (d, 3H, C*H*$_3$-NH-CO), 2.87-2.81 (m, 3H, CH_2N), 2.81-2.78 (m, 7H, CH_2N (3H), piperazine (4H)), 2.74-2.67 (m, 5H, TACN-CH_2C*H*$_2$-Ph (2H), CH_2N (3H)), 2.63-2.49 (m, 3H, TACN-C*H*$_2$$CH_2$-Ph (2H), CH_2N (1H)), 1.56-1.40 (m, 27H, Boc), 1.34, 1.26-1.20 (m, 2H, cyclopropane CH_2), 1.10-1.09 (m, 2H, cyclopropane CH_2); ^{13}C NMR (150 MHz, $CDCl_3$) δ_C 175.04 (cipro C=O), 165.02 (cipro C=O), 162.89 (guanidine C), 162.18, 158.07 (Boc C=O), 154.26 (Boc C=O), 152.88 (cipro), 152.16 (Boc C=O), 147.12 (cipro C-H), 145.26 (cipro), 142.34 (linker Ar), 140.99, 137.99 (cipro), 134.88 (linker Ar), 132.85, 129.66, 128.24 (C-H linker Ar), 127.33, 125.38 (C-H linker Ar), 123.00 (cipro), 112.31 (cipro C-H), 111.12 (cipro), 104.28 (cipro C-H), 89.15 (Boc *C*$(CH_3)_3$), 83.68 (Boc *C*$(CH_3)_3$), 79.35 (Boc *C*$(CH_3)_3$), 62.65 (Ph-*C*H_2-piperazine), 58.91, 57.74, 54.68, 54.34, 53.98, 53.65, 53.09 (*C*H_2N), 52.89 (piperazine), 50.37 (*C*H_2N), 49.56 (piperazine), 48.88, 47.85 (*C*H_2N), 42.48, 39.51, 38.26 (*C*H_2-guanidine), 36.63 (cyclopropane *C*H), 34.05 (TACN-CH_2*C*H_2-Ph), 33.86, 28.63 (Boc C(*C*$H_3)_3$), 28.01 (Boc C(*C*$H_3)_3$), 27.93 (Boc C(*C*$H_3)_3$), 26.02 (*C*H_3-NH-CO), 7.08

(cyclopropane <u>*C*</u>H_2). MS (ESI+ QTOFMS) calculated for $C_{51}H_{76}FN_{10}O_8$ ($[M+H]^+$) *m/z* 975.53; measured *m/z* 975.65.

Compound 14c

Following the general procedure, compounds **13c** (0.411 g, 0.550 mmol) and N,N-di-Boc-1H-pyrazole-1-carboxamidine (0.171 g, 0.550 mmol) yielded 53% of compound **14c** (0.544 g, 0.550 mmol);

^{1}H NMR (600 MHz, $CDCl_3$) δ_H 11.50 (d, 1H, Boc-N<u>*H*</u>-guanidine), 9.91 (q, 1H, CH_3-N<u>*H*</u>-CO), 8.83 (s, 1H, QH-2), 8.76-8.68 (m, 1H, guanidine N<u>*H*</u>), 8.03 (d, 1H, QH-5), 7.33 (d, 1H, QH-8), 7.28-7.25 (m, 2H, linker Ar), 7.17 (d, 2H, linker Ar), 3.58 (s, 2H, Ph-C<u>*H*$_2$</u>-piperazine), 3.53-3.37 (m, 7H, C<u>*H*$_2$</u>-guanidine (2H), cyclopropane CH (1H), CH_2N (4H)), 3.35-3.28 (m, 4H, piperazine), 3.01 (d, 3H, C<u>*H*$_3$</u>-NH-CO), 2.98-2.89 (m, 3H, CH_2N), 2.89-2.84 (m, 1H, CH_2N), 2.75-2.71 (m, 2H, CH_2N), 2.71-2.67 (m, 4H, piperazine), 2.66-2.61 (m, 5H, TACN-$(CH_2)_2$C<u>*H*$_2$</u>-Ph (2H), CH_2N (3H)), 2.61-2.54 (m, 3H, TACN-C<u>*H*$_2$</u>$(CH_2)_2$-Ph (2H), CH_2N (1H)), 1.82-1.72 (m, 2H, TACN-CH_2C<u>*H*$_2$</u>CH_2-Ph), 1.52 (s, 9H, Boc), 1.49 (s, 9H, Boc), 1.46 (s, 9H, Boc), 1.35-1.30 (m, 2H, cyclopropane CH_2), 1.19-1.13 (m, 2H, cyclopropane CH_2); ^{13}C NMR (150 MHz, $CDCl_3$) δ_C 175.47 (cipro C=O), 165.62 (cipro C=O), 163.59 (guanidine C), 156.08, 156.05 (Boc C=O), 155.49, 155.31 (Boc C=O), 153.43 (cipro), 152.96 (Boc C=O), 146.52 (cipro C-H), 145.03 (cipro), 141.57, 141.41 (linker Ar), 138.46 (cipro), 134.98, 134.92 (linker Ar), 129.25, 129.22 (C-H linker Ar), 128.36, 128.33 (C-H linker Ar), 121.72 (cipro), 112.51 (cipro C-H), 111.36 (cipro), 104.66 (cipro C-H), 82.89 (Boc <u>*C*</u>$(CH_3)_3$), 82.75 (Boc <u>*C*</u>$(CH_3)_3$), 79.22 (Boc <u>*C*</u>$(CH_3)_3$), 62.72 (Ph-<u>*C*</u>H_2-piperazine), 57.51, 57.37, 57.06, 56.89, 56.02, 55.91, 55.66, 55.34, 55.08, 54.15, 53.15 (<u>*C*</u>H_2N), 52.75 (piperazine), 50.23 (<u>*C*</u>H_2N), 50.02 (piperazine), 49.82, 49.04, 48.88 (<u>*C*</u>H_2N), 39.31, 39.19 (<u>*C*</u>H_2-guanidine), 34.63 (cyclopropane <u>*C*</u>H), 33.42, 33.33 (TACN-$(CH_2)_2$<u>*C*</u>H_2-Ph), 28.59 (Boc C(<u>*C*</u>$H_3)_3$), 28.45 (TACN-CH_2<u>*C*</u>H_2CH_2-Ph), 28.31 (Boc C(<u>*C*</u>$H_3)_3$), 28.07 (Boc C(<u>*C*</u>$H_3)_3$), 25.83 (<u>*C*</u>H_3-NH-CO), 8.19 (cyclopropane <u>*C*</u>H_2). MS (ESI+ QTOFMS) calculated for $C_{52}H_{78}FN_{10}O_8$ ($[M+H]^+$) *m/z* 989.60; measured *m/z* 989.55.

Compound 14d

Following the general procedure, compounds **13d** (0.974 g, 1.28 mmol) and N,N-di-Boc-1H-pyrazole-1-carboxamidine (0.397 g, 1.28 mmol) yielded 49% of compound **14d** (0.630 g, 0.628 mmol);

^{1}H NMR (600 MHz, $CDCl_3$) δ_H 11.45 (d, 1H, Boc-N<u>*H*</u>-guanidine), 9.84 (q, 1H, CH_3-N<u>*H*</u>-CO), 8.76 (s, 1H, QH-2), 8.47 (m, 1H, guanidine N<u>*H*</u>), 7.97-7.94 (d, 1H, QH-5), 7.56 (d, 1H, QH-8), 7.26-7.23 (m, 2H, linker Ar), 7.08-7.07 (d, 2H, linker Ar), 3.53 (s, 2H, Ph-C<u>*H*$_2$</u>-piperazine), 3.42-3.37 (m, 6H, C<u>*H*$_2$</u>-guanidine (2H), CH_2N (4H)), 3.35-3.28 (m, 5H, piperazine(4H), cyclopropane CH (1H)), 2.93 (d, 3H, C<u>*H*$_3$</u>-NH-CO), 2.68-2.50 (m, 18H, CH_2N(10H), piperazine (4H)), TACN-$(CH_2)_3$C<u>*H*$_2$</u>-Ph (2H), TACN-C<u>*H*$_2$</u>$(CH_2)_3$-Ph (2H)), 1.64-1.52 (m, 4H, TACN-CH_2(C<u>*H*$_2$</u>$)_2CH_2$-Ph), 1.45-1.41 (s, 27H, Boc), 1.25-1.23 (m, 2H, cyclopropane CH_2), 1.10-1.07 (m, 2H, cyclopropane CH_2); ^{13}C NMR (150 MHz, $CDCl_3$) δ_C 174.89 (cipro C=O), 163.84 (cipro C=O), 162.01 (guanidine C), 157.92, 158.12 (Boc C=O), 154.99 (Boc C=O),

154.01 (cipro), 153.24 (Boc C=O), 147.22 (cipro C-H), 144.85 (cipro), 140.34 (linker Ar), 139.56, 138.84 (cipro), 135.92 (linker Ar), 133.54, 128.27 (C-H linker Ar), 126.30 (C-H linker Ar), 124.86, 120.80 (cipro), 111.41 (cipro C-H), 109.29 (cipro), 104.02 (cipro C-H), 83.01 (Boc $\underline{C}(CH_3)_3$), 81.78 (Boc $\underline{C}(CH_3)_3$), 77.25 (Boc $\underline{C}(CH_3)_3$), 64.79 (Ph-$\underline{C}H_2$-piperazine), 59.31, 57.91, 55.68, 54.10, 52.18 ($\underline{C}H_2N$), 51.95 (piperazine), 51.27 ($\underline{C}H_2N$), 50.88 (piperazine), 49.58, 47.92 ($\underline{C}H_2N$), 39.69 ($\underline{C}H_2$-guanidine), 38.05, 37.05, 35.74 (cyclopropane $\underline{C}H$), 35.08 (TACN-$(CH_2)_3\underline{C}H_2$-Ph), 29.03 (Boc C($\underline{C}H_3)_3$), 28.87-28.79 (TACN-$CH_2(\underline{C}H_2)_2CH_2$-Ph), 28.65 (Boc C($\underline{C}H_3)_3$), 28.11 (Boc C($\underline{C}H_3)_3$), 23.86 ($\underline{C}H_3$-NH-CO), 8.22 (cyclopropane $\underline{C}H_2$). MS (ESI+ QTOFMS) calculated for $C_{52}H_{78}FN_{10}O_8$ ($[M+H]^+$) *m/z* 1003.61; measured *m/z* 1003.78.

3. ^{1}H and ^{13}C NMR spectra of compounds **1-8**

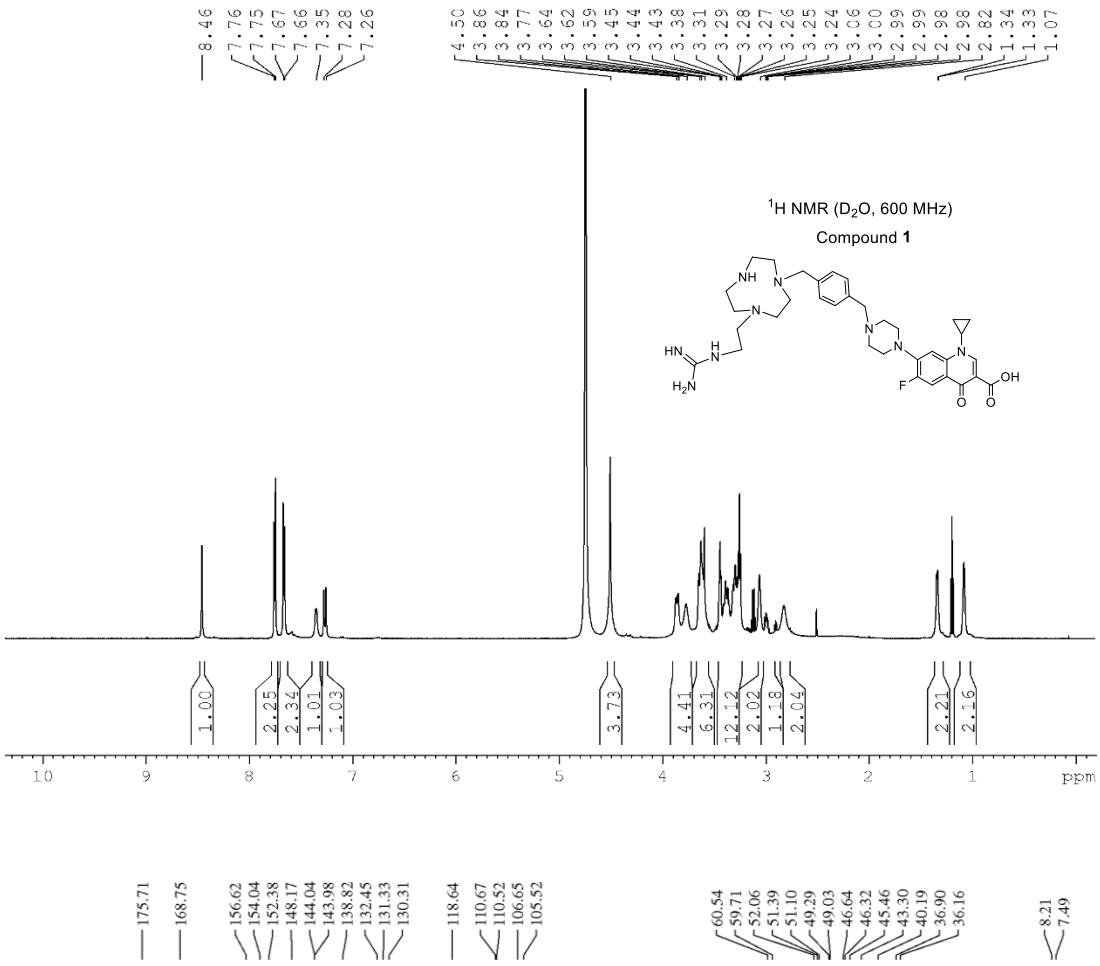

^{1}H NMR (D_2O, 600 MHz)

Compound **1**

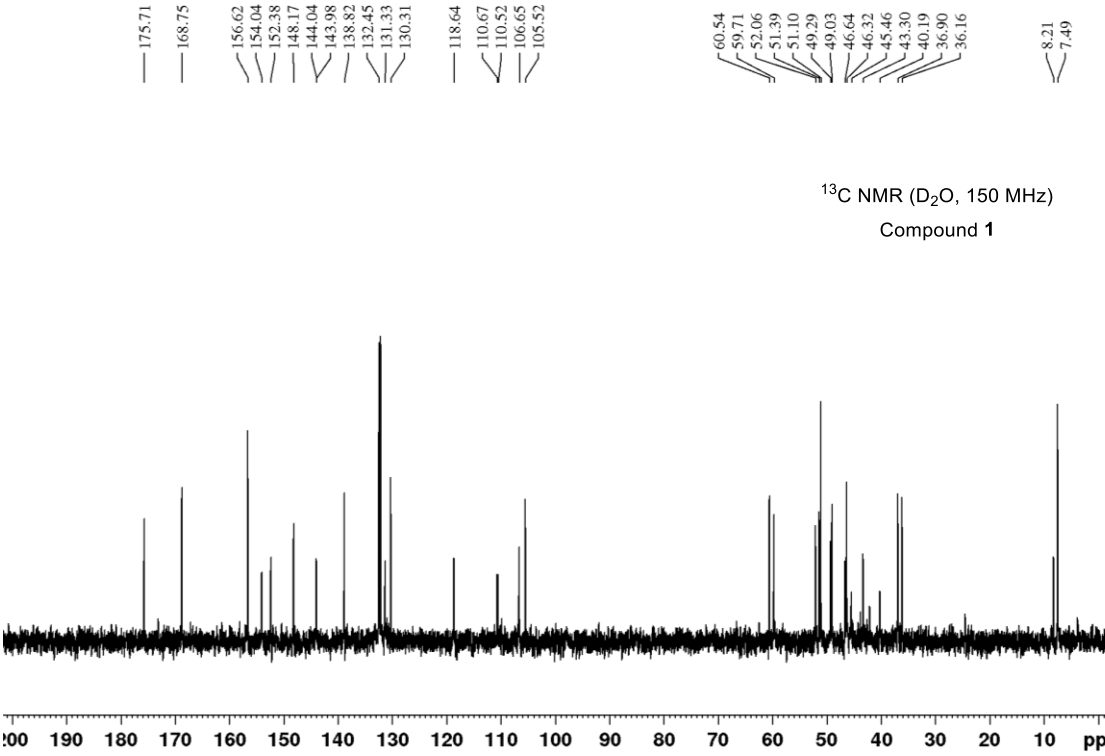

^{13}C NMR (D_2O, 150 MHz)

Compound **1**

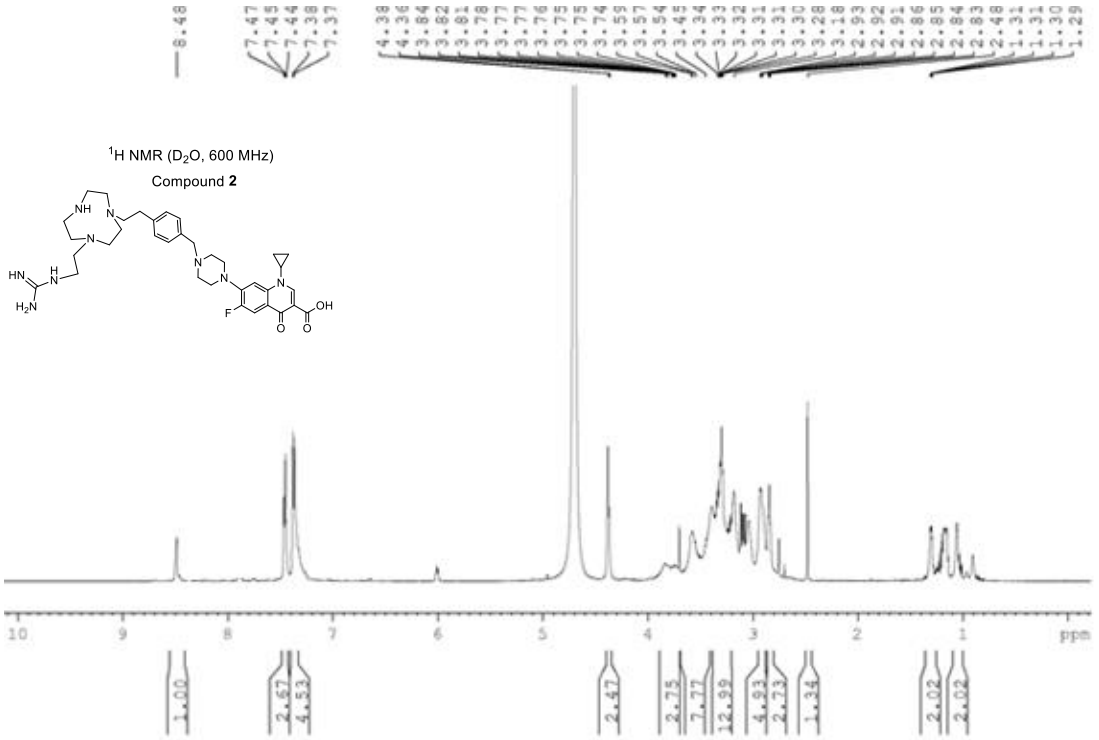
^{1}H NMR (D_2O, 600 MHz)
Compound **2**

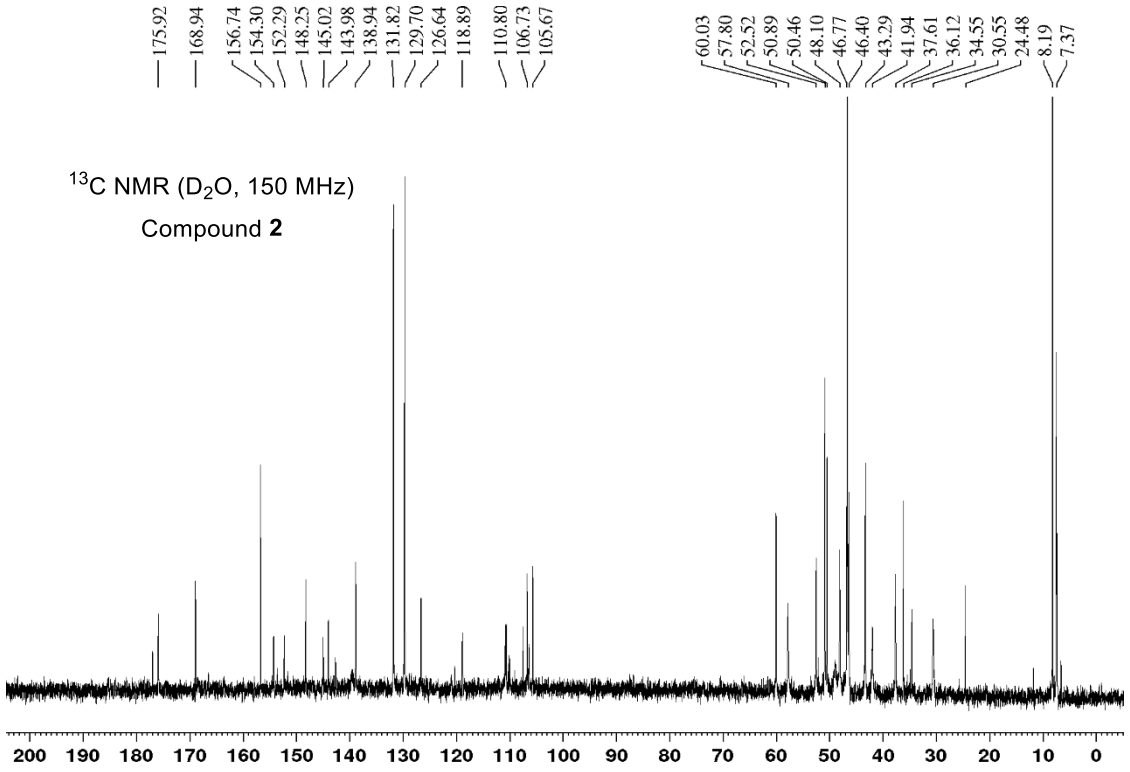
^{13}C NMR (D_2O, 150 MHz)
Compound **2**

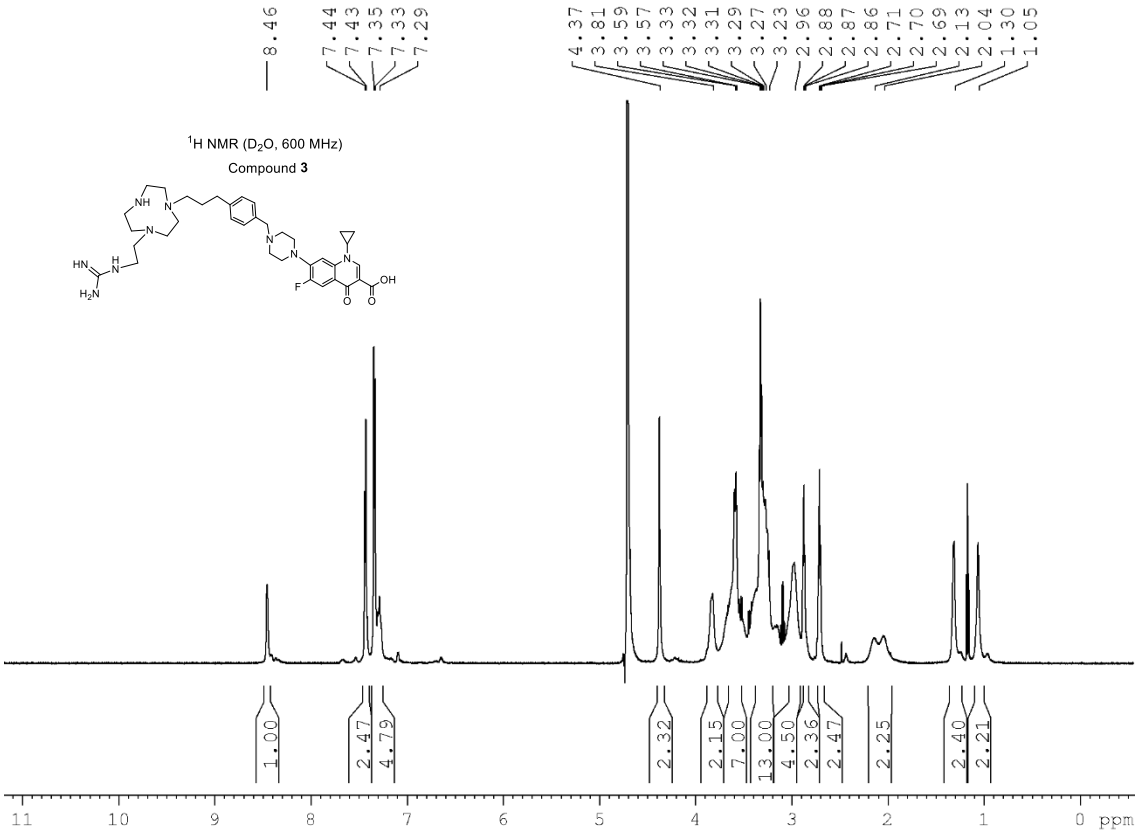
8.46
7.44
7.43
7.35
7.33
7.29
4.37
3.81
3.59
3.57
3.33
3.32
3.31
3.29
3.27
3.23
2.96
2.88
2.87
2.86
2.71
2.70
2.69
2.13
2.04
1.30
1.05
1H NMR (D2O, 600 MHz)
Compound 3
1.00
2.47
4.79
2.32
2.15
7.00
13.00
4.50
2.36
2.47
2.25
2.40
2.21
11
10
9
8
7
6
5
4
3
2
1
0 ppm

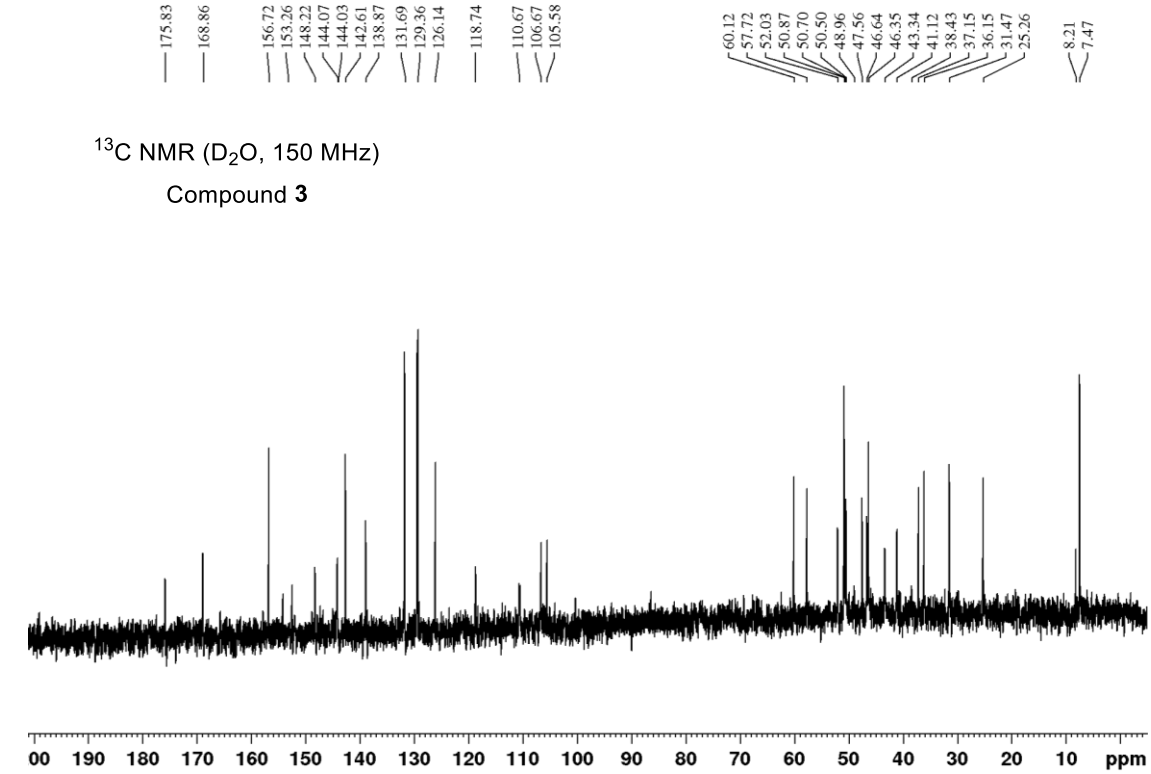
175.83
168.86
156.72
153.26
148.22
144.07
144.03
142.61
138.87
131.69
129.36
126.14
118.74
110.67
106.67
105.58
60.12
57.72
52.03
50.87
50.70
50.50
48.96
47.56
46.64
46.35
43.34
41.12
38.43
37.15
36.15
31.47
25.26
8.21
7.47
13C NMR (D2O, 150 MHz)
Compound 3
00
190
180
170
160
150
140
130
120
110
100
90
80
70
60
50
40
30
20
10
ppm

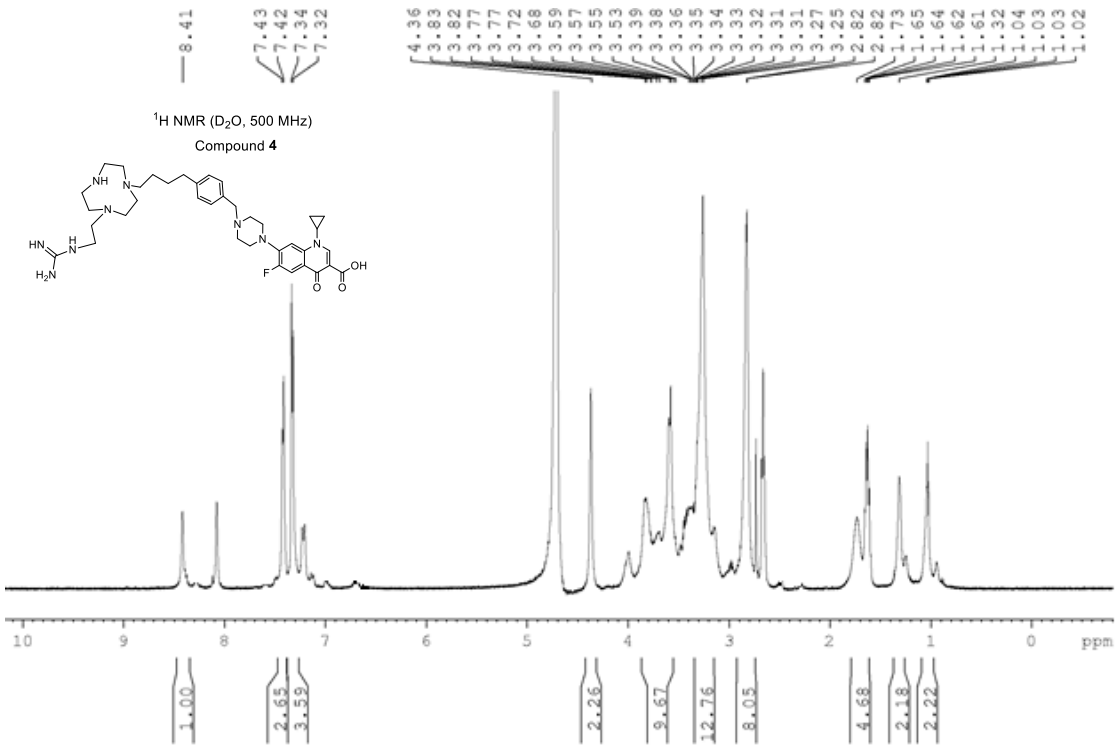

^{1}H NMR (D_2O, 500 MHz)

Compound **4**

^{13}C NMR (D_2O, 126 MHz)

Compound **4**

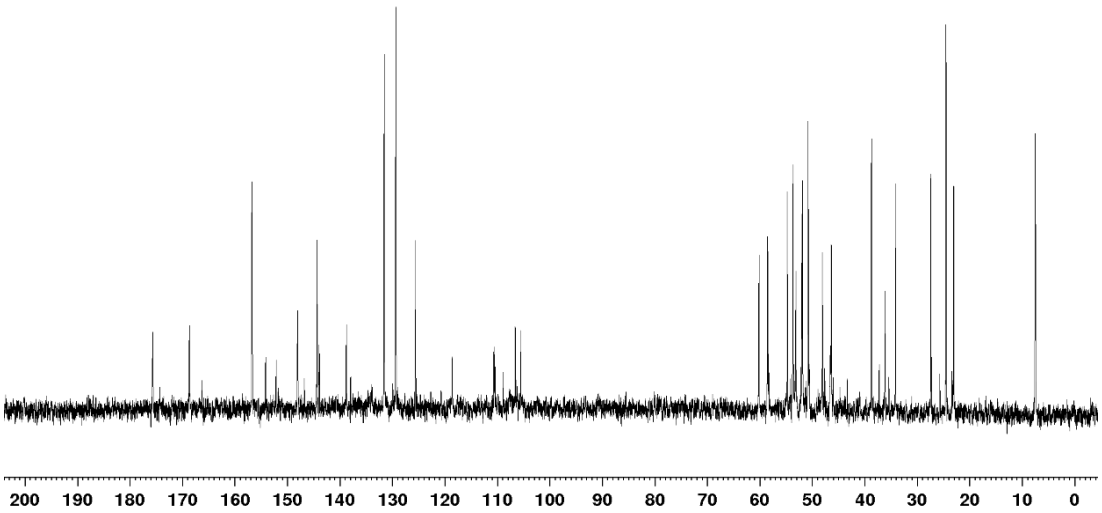

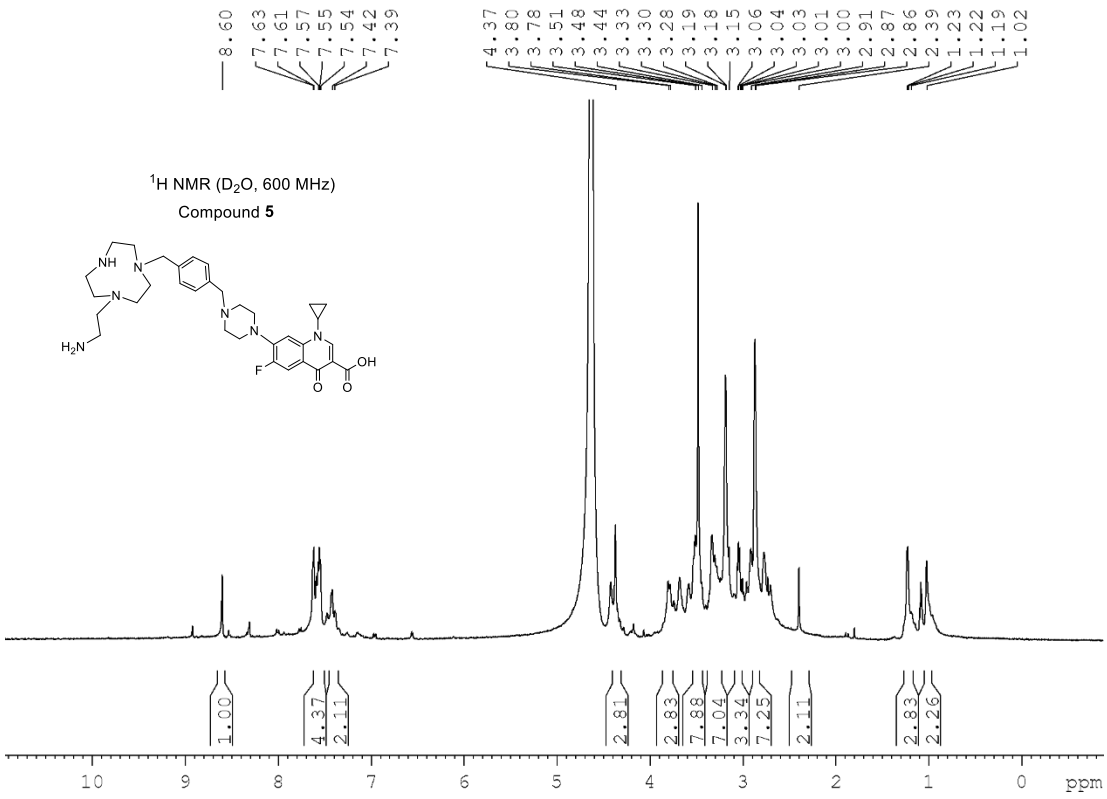
8.60
7.63
7.61
7.57
7.55
7.54
7.42
7.39
4.37
3.80
3.78
3.51
3.48
3.44
3.33
3.30
3.28
3.19
3.18
3.15
3.06
3.04
3.03
3.01
3.00
2.91
2.87
2.86
2.39
1.23
1.22
1.19
1.02
1H NMR (D2O, 600 MHz)
Compound 5
1.00
4.37
2.11
2.81
2.83
7.88
7.04
3.34
7.25
2.11
2.83
2.26
10
9
8
7
6
5
4
3
2
1
0
ppm

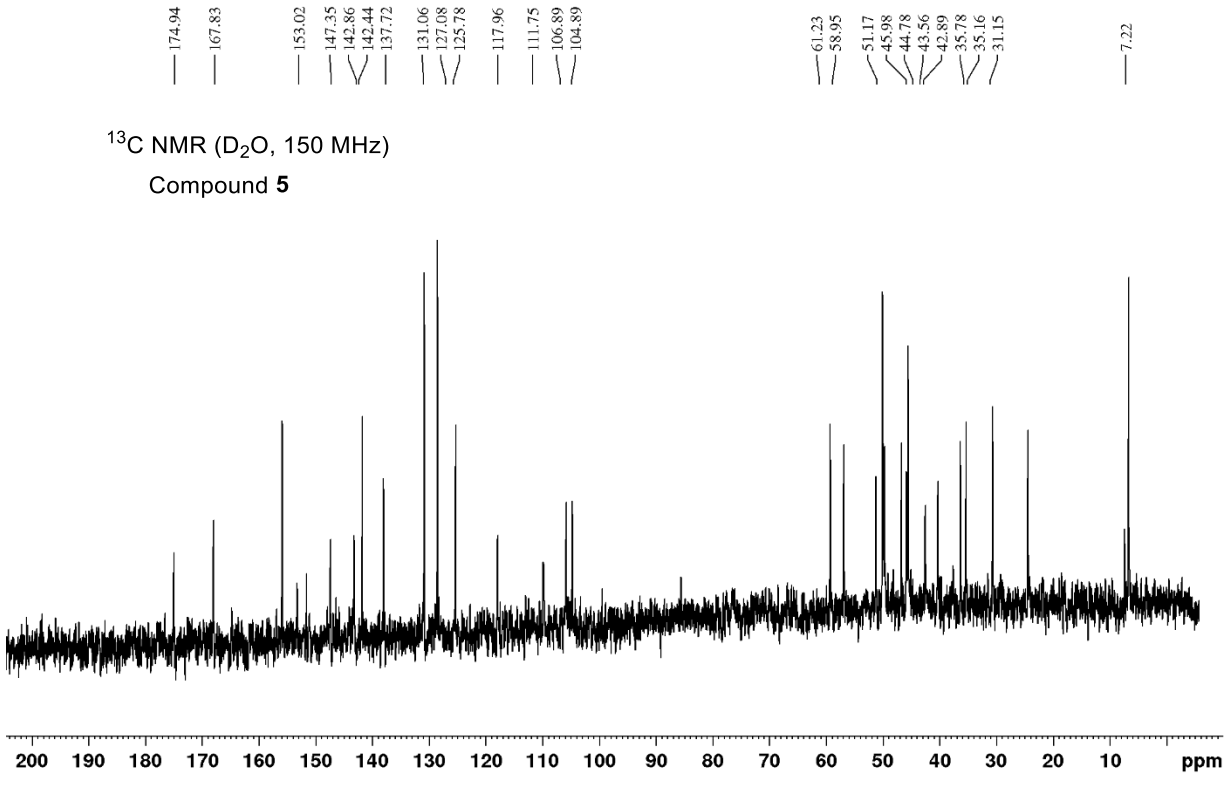
174.94
167.83
153.02
147.35
142.86
142.44
137.72
131.06
127.08
125.78
117.96
111.75
106.89
104.89
61.23
58.95
51.17
45.98
44.78
43.56
42.89
35.78
35.16
31.15
7.22
13C NMR (D2O, 150 MHz)
Compound 5
200
190
180
170
160
150
140
130
120
110
100
90
80
70
60
50
40
30
20
10
ppm

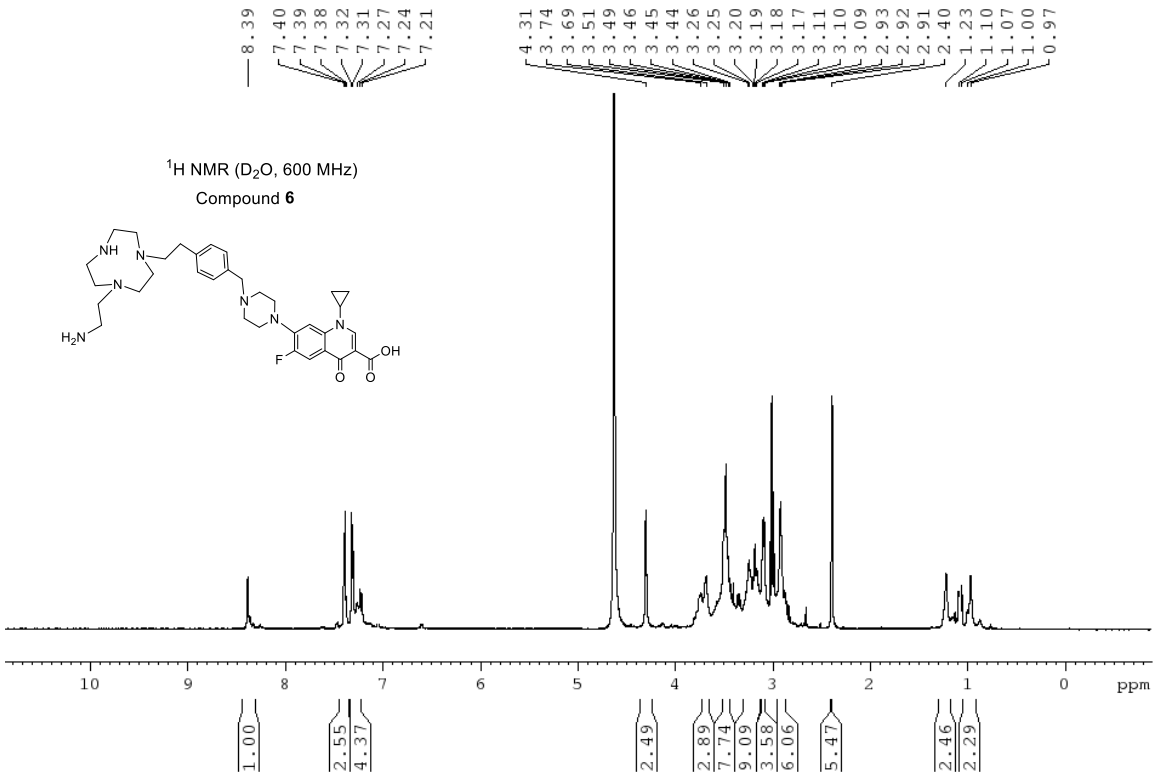
8.39
7.40
7.39
7.38
7.32
7.31
7.27
7.24
7.21
4.31
3.74
3.69
3.51
3.49
3.46
3.45
3.44
3.26
3.25
3.20
3.19
3.18
3.17
3.11
3.10
3.09
2.93
2.92
2.91
2.40
1.23
1.10
1.07
1.00
0.97
1H NMR (D2O, 600 MHz)
Compound 6
NH
N
N
N
N
H2N
F
OH
O
O
10
9
8
7
6
5
4
3
2
1
0
ppm
1.00
2.55
4.37
2.49
2.89
7.74
9.09
3.58
6.06
5.47
2.46
2.29

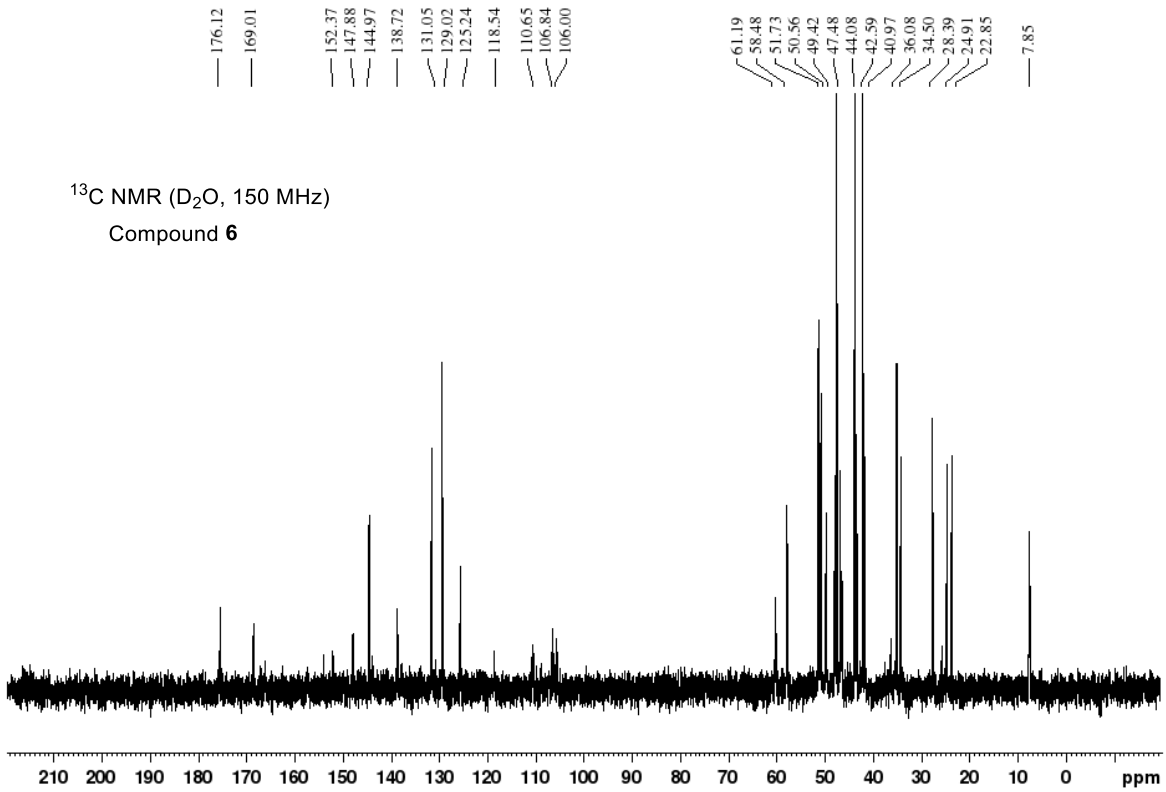
176.12
169.01
152.37
147.88
144.97
138.72
131.05
129.02
125.24
118.54
110.65
106.84
106.00
61.19
58.48
51.73
50.56
49.42
47.48
44.08
42.59
40.97
36.08
34.50
28.39
24.91
22.85
7.85
13C NMR (D2O, 150 MHz)
Compound 6
210
200
190
180
170
160
150
140
130
120
110
100
90
80
70
60
50
40
30
20
10
0
ppm

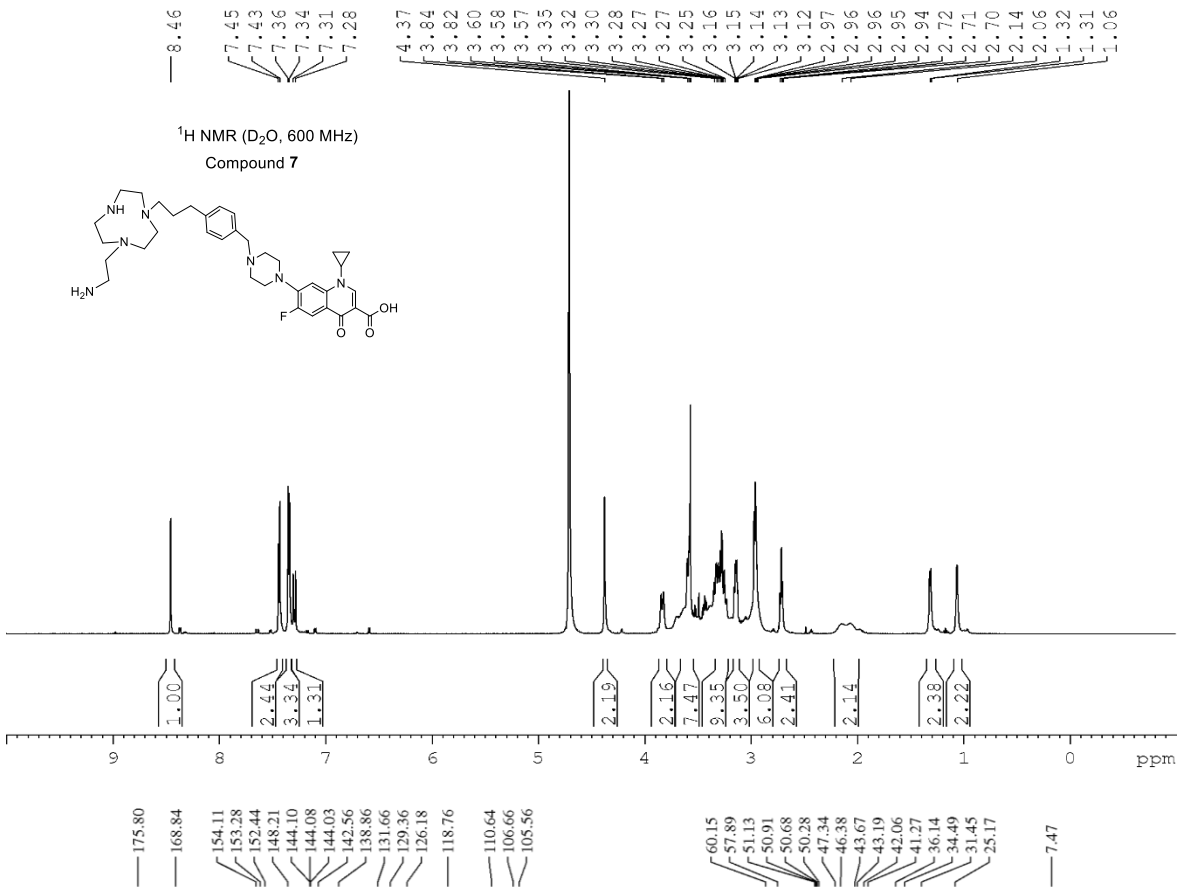

^{1}H NMR (D_2O, 600 MHz)

Compound **7**

^{13}C NMR (D_2O, 150 MHz)

Compound **7**

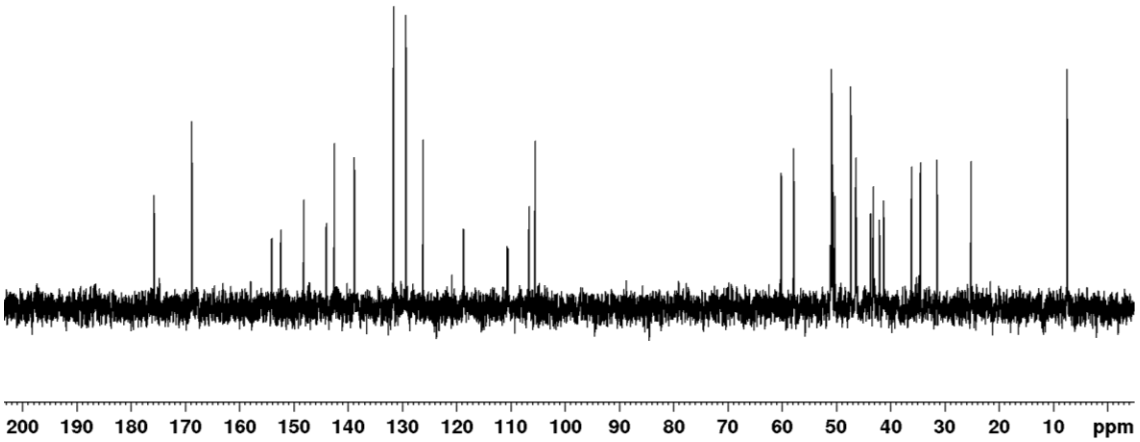

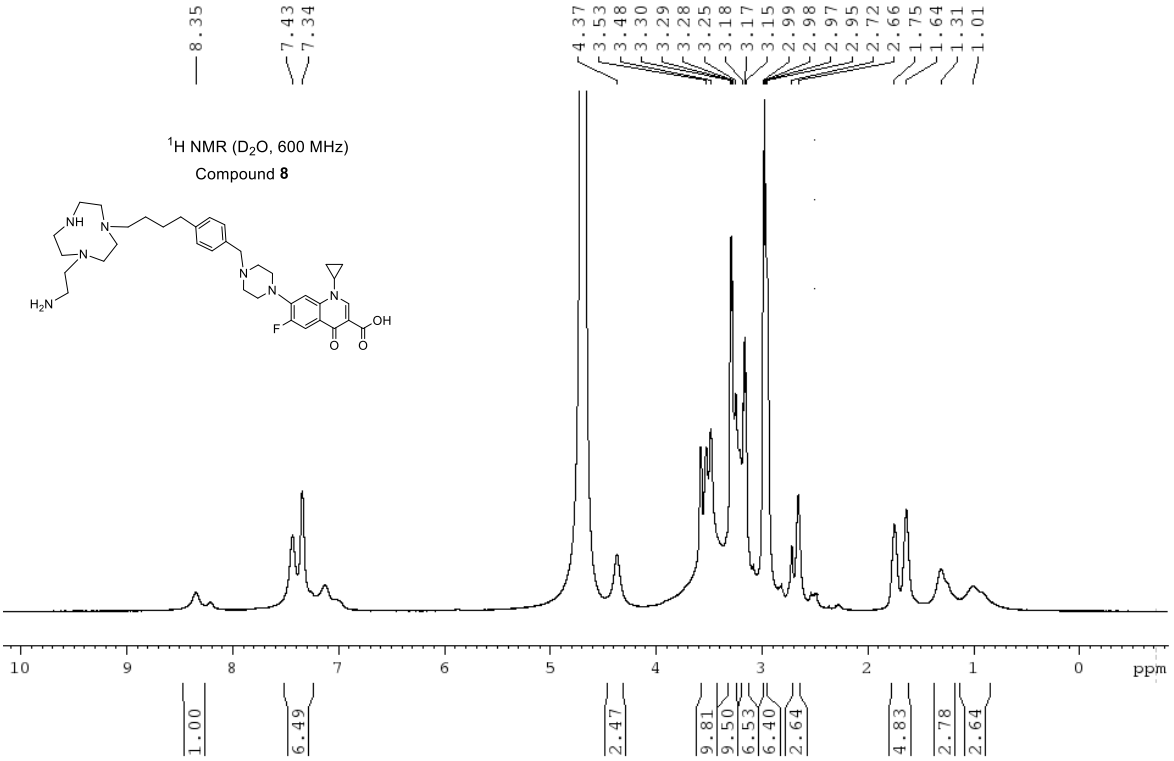
8.35
7.43
7.34
4.37
3.53
3.48
3.30
3.29
3.28
3.25
3.18
3.17
3.15
2.99
2.98
2.97
2.95
2.72
2.66
1.75
1.64
1.31
1.01
1H NMR (D2O, 600 MHz)
Compound 8
NH
N
N
N
N
H2N
F
N
OH
O
O
10
9
8
7
6
5
4
3
2
1
0
ppm
1.00
6.49
2.47
9.81
9.50
6.53
6.40
2.64
4.83
2.78
2.64

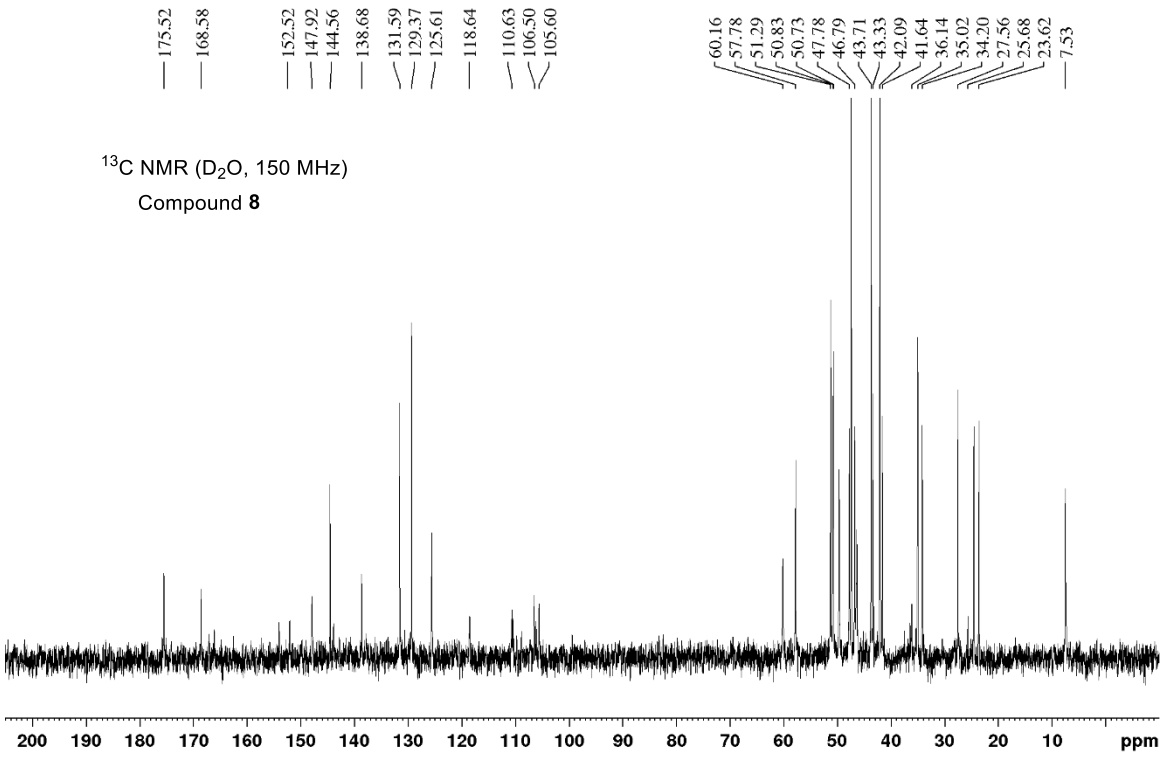
175.52
168.58
152.52
147.92
144.56
138.68
131.59
129.37
125.61
118.64
110.63
106.50
105.60
60.16
57.78
51.29
50.83
50.73
47.78
46.79
43.71
43.33
42.09
41.64
36.14
35.02
34.20
27.56
25.68
23.62
7.53
13C NMR (D2O, 150 MHz)
Compound 8
200
190
180
170
160
150
140
130
120
110
100
90
80
70
60
50
40
30
20
10
ppm

4. HRMS data for Cu(II) complexes

Compound **1**-Cu(II)

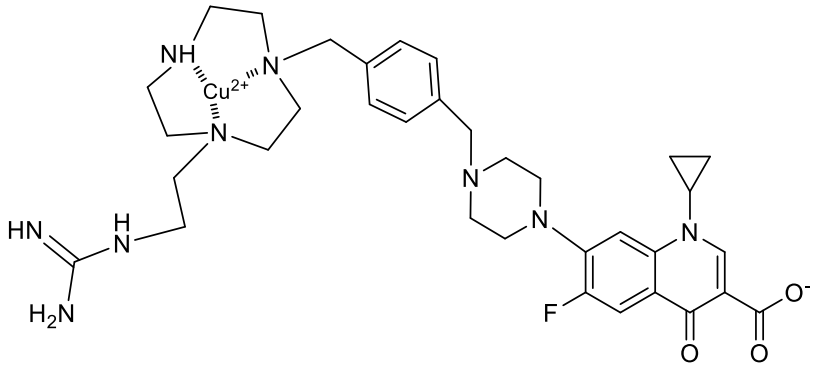

Chemical Formula: $C_{34}H_{45}CuFN_9O_3^+$

Exact Mass: 709.29

Data from HRMS : **709.2921**

Elemental Composition Report **Page 1**

Single Mass Analysis
Tolerance = 40.0 mDa / DBE: min = -1.5, max = 200.0
Element prediction: Off
Number of isotope peaks used for i-FIT = 3

Monoisotopic Mass, Even Electron Ions
8 formula(e) evaluated with 1 results within limits (up to 50 closest results for each mass)
Elements Used:
C: 33-35 H: 44-46 N: 8-10 O: 2-3 Cu: 0-2 F: 0-2

709.2921 (^{63}Cu-69.15%)

711.2901 (^{65}Cu-30.85%)

Fc1
Ba_9573 42 (0.244) Cm (22:39)
1: TOF MS ES+
8.34e+005

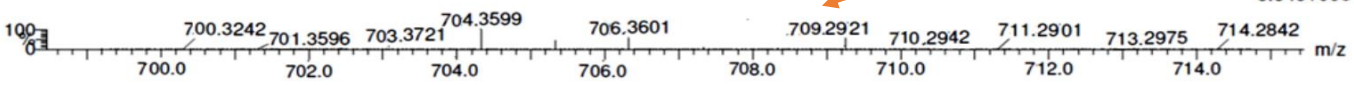

Minimum:				-1.5				
Maximum:		40.0	10.0	200.0				
Mass	Calc. Mass	mDa	PPM	DBE	i-FIT	Norm	Conf(%)	Formula
709.2921	709.2920	-0.1	-0.1	16.5	530.4	n/a	n/a	C34 H45 N9 O3 Cu F

Cu Isotope distribution : 709.2921 (^{63}Cu-69.15%), 711.2901 (^{65}Cu-30.85%)

Compound **2**-Cu(II)

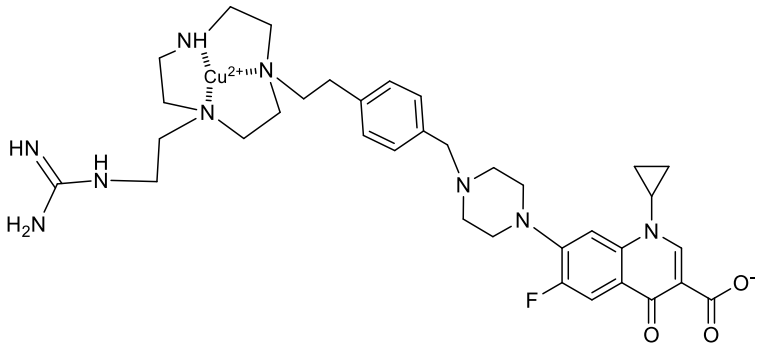

A name could not be generated for this structure.

Chemical Formula: $C_{35}H_{47}CuFN_9O_3^+$

Exact Mass: 723.31

Data from HRMS : **723.3070**

Elemental Composition Report **Page 1**

Single Mass Analysis

Tolerance = 40.0 mDa / DBE: min = -1.5, max = 200.0

Element prediction: Off

Number of isotope peaks used for i-FIT = 3

Monoisotopic Mass, Odd and Even Electron Ions

12 formula(e) evaluated with 1 results within limits (up to 50 closest results for each mass)

Elements Used:

C: 34-36 H: 46-48 N: 8-10 O: 2-4 F: 0-2 Cu: 0-2

R135

Ba_9496 29 (0.237) Cm (17:31)

723.3070 (100%, ^{63}Cu-69.15%)

725.3054 (44.6%, ^{65}Cu-30.85%)

1: TOF MS ES+
3.45e+005

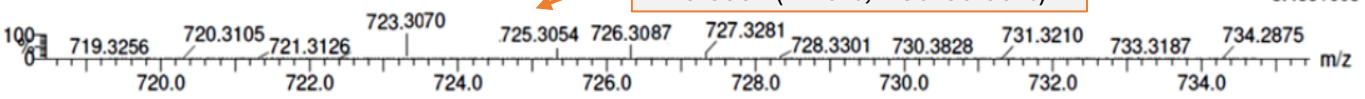

Minimum:				-1.5				
Maximum:		40.0	10.0	200.0				
Mass	Calc. Mass	mDa	PPM	DBE	i-FIT	Norm	Conf(%)	Formula
723.3070	723.3076	0.3	0.4	15.5	528.5	n/a	n/a	C35 H47 N9 O3 F Cu

Cu Isotope distribution : 723.3070 (100%, ˜˜Cu-69.15%), 725.3054 (˜˜Cu-30.85%)

Compound **3**-Cu(II)

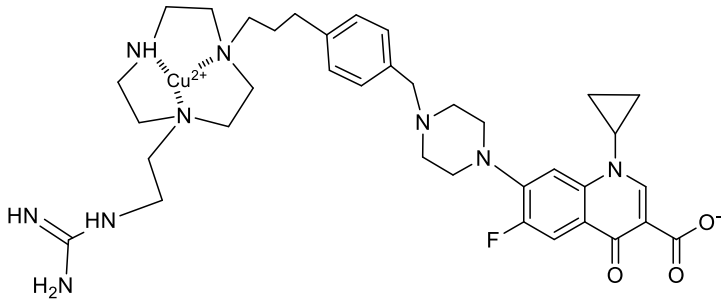

Chemical Formula: $C_{36}H_{49}CuFN_9O_3^+$

Exact Mass: 737.32

Data from HRMS : **737.3230**

Elemental Composition Report **Page 1**

Single Mass Analysis

Tolerance = 40.0 mDa / DBE: min = -1.5, max = 200.0

Element prediction: Off

Number of isotope peaks used for i-FIT = 3

Monoisotopic Mass, Even Electron Ions

4 formula(e) evaluated with 1 results within limits (up to 50 closest results for each mass)

Elements Used:

C: 35-37 H: 48-50 N: 8-10 O: 2-4 F: 0-1 Cu: 0-1

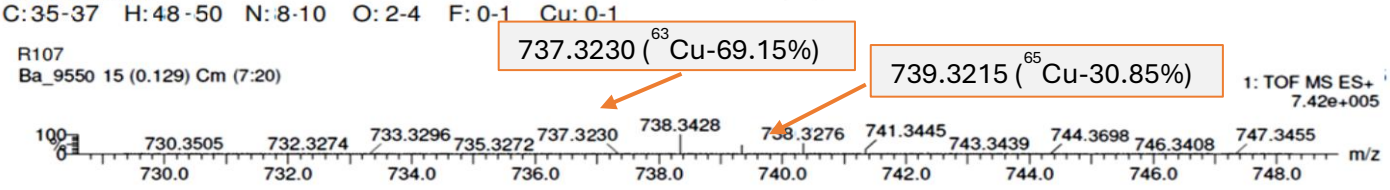

Minimum:				-1.5				
Maximum:		40.0	10.0	200.0				
Mass	Calc. Mass	mDa	PPM	DBE	i-FIT	Norm	Conf(%)	Formula
737.3230	737.3233	0.9	1.2	16.5	390.5	n/a	n/a	C36 H49 N9 O3 F Cu

Cu Isotope distribution : 737.3230 (^{63}Cu-69.15%), 739.3215 (^{65}Cu-30.85%)

Compound **4**-Cu(II)

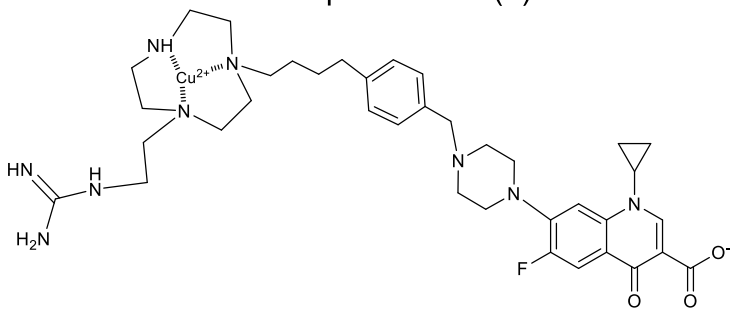

Chemical Formula: $C_{37}H_{51}CuFN_9O_3^+$

Elemental Composition Report **Page 1**

Single Mass Analysis
Tolerance = 40.0 mDa / DBE: min = -1.5, max = 200.0
Element prediction: Off
Number of isotope peaks used for i-FIT = 3

Monoisotopic Mass, Even Electron Ions
4 formula(e) evaluated with 1 results within limits (up to 50 closest results for each mass)
Elements Used:
C: 36-38 H: 50-51 N: 8-10 O: 2-4 F: 0-1 Cu: 0-1

751.3389 (100%, ^{63}Cu-69.15%)

753.3372 (44.6%, ^{65}Cu-30.85%)

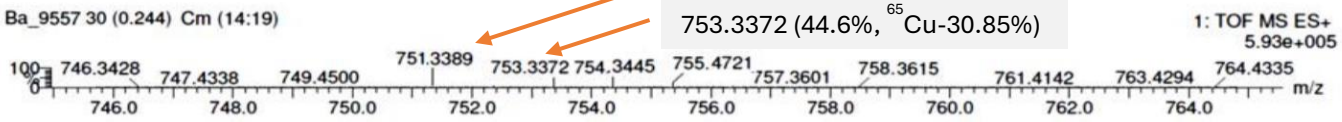

Minimum:				-1.5				
Maximum:		40.0	10.0	200.0				
Mass	Calc. Mass	mDa	PPM	DBE	i-FIT	Norm	Conf(%)	Formula
751.3389	751.3389	0.9	1.2	16.5	390.5	n/a	n/a	C37 H51 N9 O3 F Cu

Cu Isotope distribution : 751.3389 (100%, ^{63}Cu-69.15%), 753.3372 (44.6%, ^{65}Cu-30.85%)

Compound **5**-Cu(II)

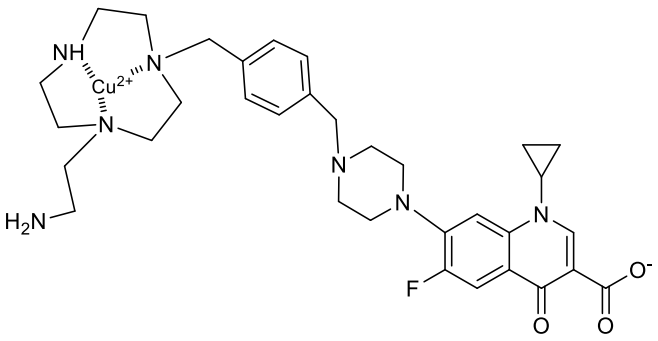

Chemical Formula: $C_{33}H_{43}CuFN_7O_3^+$

Exact Mass: 667.27

Data from HRMS :**667.2716**

Elemental Composition Report **Page 1**

Single Mass Analysis
Tolerance = 40.0 mDa / DBE: min = -1.5, max = 200.0
Element prediction: Off
Number of isotope peaks used for i-FIT = 3

Monoisotopic Mass, Even Electron Ions
12 formula(e) evaluated with 1 results within limits (up to 50 closest results for each mass)
Elements Used:
C: 32-34 H: 42-44 N: 5-15 O: 2-4 Cu: 0-2 F: 0-2

667.2716 (^{63}Cu-69.15%)

669,2739 (^{65}Cu-30.85%)

Minimum:				-1.5				
Maximum:		40.0	10.0	200.0				
Mass	Calc. Mass	mDa	PPM	DBE	i-FIT	Norm	Conf(%)	Formula
667.2716	667.2702	-1.4	-1.9	15.5	562.4	0.346	70.73	C33 H43 N7 O3 Cu F

Cu Isotope distribution : 667.2716 (^{63}Cu-69.15%), 669.2739 (^{65}Cu-30.85%)

Compound **6**-Cu(II)

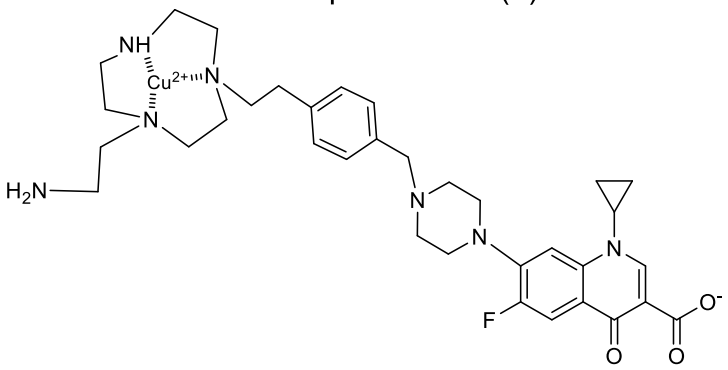

Chemical Formula: $C_{34}H_{45}CuFN_7O_3^+$

Exact Mass: 681.29

Data from HRMS : **681.2856**

Elemental Composition Report **Page 1**

Single Mass Analysis

Tolerance = 40.0 mDa / DBE: min = -1.5, max = 200.0

Element prediction: Off

Number of isotope peaks used for i-FIT = 3

Monoisotopic Mass, Even Electron Ions

8 formula(e) evaluated with 1 results within limits (up to 50 closest results for each mass)

Elements Used:

C: 33-35 H: 44-50 N: 5-10 O: 2-3 Cu: 0-2 F: 0-2

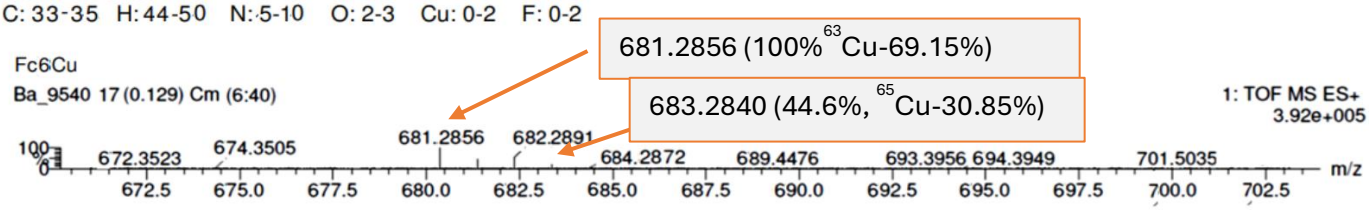

Minimum:				-1.5				
Maximum:		40.0	10.0	200.0				
Mass	Calc. Mass	mDa	PPM	DBE	i-FIT	Norm	Conf(%)	Formula
681.2856	681.2858	-0.1	-0.1	16.5	530.4	n/a	n/a	C34 H45 N7 O3 Cu F

Cu Isotope distribution : 681.2856 (^{63}Cu-69.15%), 683.2840 (^{65}Cu-30.85%)

Compound **7**-Cu(II)

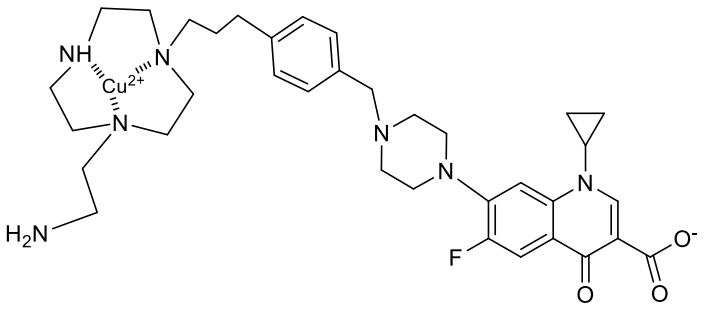

Chemical Formula: $C_{35}H_{47}CuFN_7O_3^+$

Exact Mass: 695.30

Data from HRMS : **695.3024**

Elemental Composition Report **Page 1**

Single Mass Analysis
Tolerance = 40.0 mDa / DBE: min = -1.5, max = 200.0
Element prediction: Off
Number of isotope peaks used for i-FIT = 3

Monoisotopic Mass, Even Electron Ions
5 formula(e) evaluated with 1 results within limits (up to 50 closest results for each mass)
Elements Used:
C: 34-37 H: 40-50 N: 5-10 O: 3-5 Cu: 1-1 F: 1-1

fc7-cu
Ba_9496 17 (0.237) Cm (27:29)

695.3024 (^{63}Cu-69.15%)

1: TOF MS ES+
3.33e+005

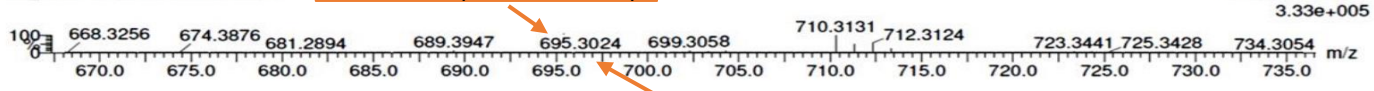

697.2997 (^{65}Cu-30.85%)

Minimum:				-1.5				
Maximum:		40.0	10.0	200.0				
Mass	Calc. Mass	mDa	PPM	DBE	i-FIT	Norm	Conf(%)	Formula
695.3024	695.3015	0.2	0.3	15.5	587.7	0.642	52.64	C35 H47 N7 O3 Cu F

Cu Isotope distribution : 695.3024 (^{63}Cu-69.15%), 697.2997 (^{65}Cu-30.85%)

Compound **8**-Cu(II)

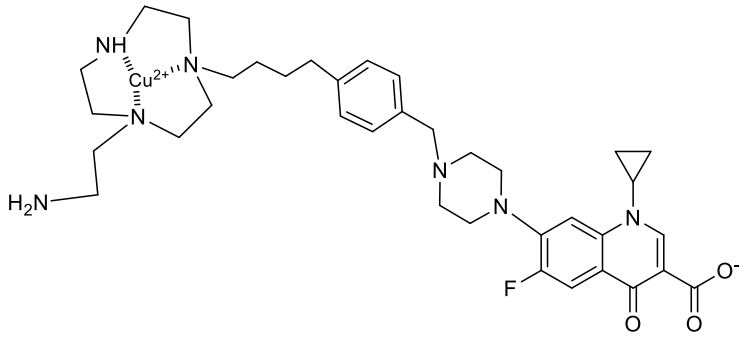

Chemical Formula: $C_{36}H_{49}CuFN_7O_3^+$

Exact Mass: 709.32

Elemental Composition Report **Page 1**

Single Mass Analysis

Tolerance = 40.0 mDa / DBE: min = -1.5, max = 200.0

Element prediction: Off

Number of isotope peaks used for i-FIT = 3

Monoisotopic Mass, Odd and Even Electron Ions

12 formula(e) evaluated with 1 results within limits (up to 50 closest results for each mass)

Elements Used:

C: 36-36 H: 48-50 N: 5-10 O: 2-4 F: 0-2 Cu: 0-2

709.3167 (^{63}Cu-69.15%)

711.3216 (^{65}Cu-30.85%)

fc 8-cu

Ba_9502 27 (0.143) Cm (27:29)

OF MS ES+

3.82e+005

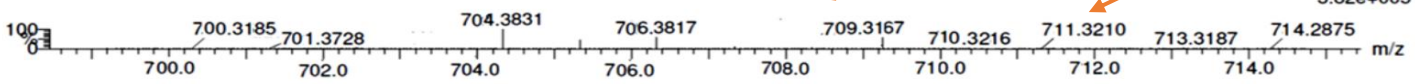

Minimum:				-1.5				
Maximum:		40.0	10.0	200.0				
Mass	Calc. Mass	mDa	PPM	DBE	i-FIT	Norm	Conf(%)	Formula
709.3167	709.3171	0.3	0.4	15.5	528.5	n/a	n/a	C36 H49 N7 O3 F Cu

Cu Isotope distribution : 709.3167 (^{63}Cu-69.15%), 711.3216 (^{65}Cu-30.85%)

17. HPLC analysis for the purity determination of compound **1**

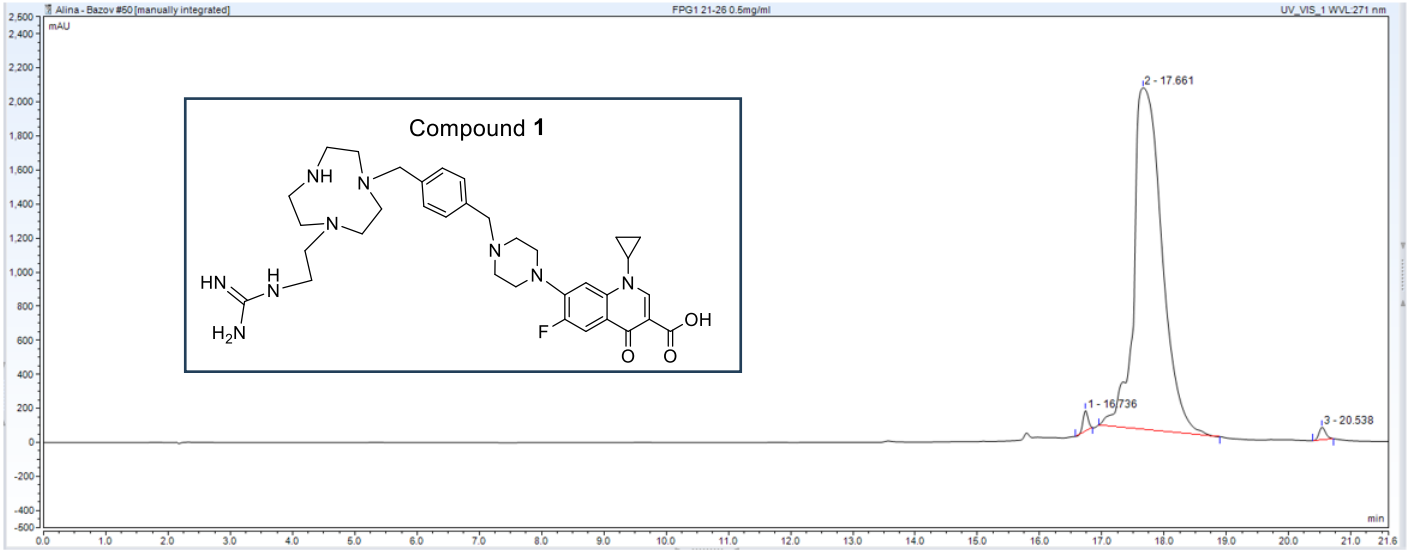

Peak No.	Peak Name	Ret.Time min	Amount n.a.	Rel.Area %	Area mAU*min	Height mAU	Type	Width (50%) min	Asym. EP	Resol. EP	Plates EP
1		16.736	n.a.	1.03	11.1319	120.73	BMB*	0.089	1.06	2.03	196455
2		17.661	n.a.	98.09	1055.9067	2005.57	BMB*	0.448	1.29	6.01	8594
3		20.538	n.a.	0.87	9.3748	74.20	BMB*	0.116	1.23	n.a.	173659
Maximum			0.0000	98.09	1055.9067	2005.57		0.448	1.29	6.01	196455
Minimum			0.0000	0.87	9.3748	74.20		0.089	1.06	2.03	8594
Sum			0.0000	100.00	1076.4134	2200.49					

HPLC analysis for the purity

Compound	Retention time (min)	% Purity
1	17.66	98.1

Method: Column Phenomenex® C18, flow 1.2 mL/min; buffer A, water 0.1% TFA; buffer B, MeCN 0.1% TFA; gradient 0-60% buffer B over 30 mins; run time, 20-30 min; injection, 200 µL of 0.1 mg/mL in water; UV detection at 271 nm.

II. Theoretical Section

1. Computational methods

1.1 Conformational analysis and determination of protonation state of TACN-guanidine warhead at physiological pH

1.1.1 Quantum chemical calculations in implicit solvation

The initial structure of the catalytic warhead was built based on the crystal structure of the Cu(II) complex of TACN with guanidinoethyl pendant[1]. At the secondary amine, an ethyl group was attached to mimic the linker as in compound **1**. All possible protonation states, from fully deprotonated to quadruple protonated, were generated. To find the most favorable isomer and conformation of each protonation state, conformational analysis using the iMTD-sMTD algorithm implemented in CREST 2.11[2] was performed. The energy of the conformers was calculated with the semi-empirical potential GFN2-xTB[3] and ALPB solvation model[4] as an aqueous solution. Subsequently, using CENSO 1.2.0[5] and Orca 5.04[6], the conformers were prescreened via single-point energy calculations at the ALPB/B97-d3/def2-SV(P) level of theory with relative energy threshold of 4 kcal/mol. Further, they were preoptimized at R2SCAN-3c and finally optimized in gas-phase at the BP86/def2-TZVP level of theory. Thermostatistical contribution was calculated under standard conditions using rigid-rotor-harmonic-oscillator approximation (RRHO). No imaginary frequencies were detected, which proves that the conformers correspond to the true energy minima on the potential energy surface. At the obtained geometries solvation free energy was calculated at BP86/def2-TZVPD using COSMO-RS model implemented in OpenCOSMO-RS[7] and Orca 6.0. The most stable isomers and conformers in each protonation state were reoptimized at BP86/def2-TZVPD in gas-phase. At the final geometries, the free energy in gas-phase and the solvation free energy were calculated and used for pK_a estimations.

1.1.2 Calculations of pK_a of TACN-guanidine warhead's amines in water

For a protonated base, a deprotonation reaction in water is as follows:

$$BH^+_{(w)} \leftrightarrow B_{(w)} + H^+_{(w)}$$

The Gibbs free energy of the reaction is related to dissociation constant as follows:

$$\Delta G_{(w)} = -RTlnK_a = -2.303RTlogK_a$$

Then, pK_a, defined as the negative logarithm of dissociation constant, is given by:

$$pK_a = \Delta G_{(w)} 2.303RT$$

where $\Delta G_{(w)}$ is the Gibbs free energy of the deprotonation reaction in the aqueous solution, R is gas constant, and T is temperature. The Gibbs free energy of the deprotonation reaction in solution can be calculated using thermodynamic cycle in which Gibbs free energies of the substrates and products are separated into gas-phase and solution contributions[8].

$$\Delta G_{(w)} = G_{(g)}(B) + \Delta G_s(B) + G_{(g)}(H^+) + \Delta G_s(H^+) + \Delta G^{1atm \to 1M} - G_{(g)}(BH^+) - \Delta G_s(BH^+)$$

The Gibbs free energies in gas-phase and Gibbs free energies of solvation of *B* and BH^+ were computed using openCOSMO-RS-DFT calculations (see Subsection 1.1.1). The gas-phase standard Gibbs free energy of a proton is -6.287 kcal/mol at 298.15 K, derived from the equation:

$$G_{(g)}(H^+) = H_{(g)}(H^+) - TS_{(g)}(H^+)$$

where $H_{(g)}(H^+) = 5/2RT$ = 1.48 kcal/mol and $S_{(g)}(H^+)$ = 26.05 cal/mol·K. The Gibbs free energy of solvation of a proton in water $\Delta G_s(H^+)$ is -265.9 kcal/mol[9]. The Gibbs free energy of the reaction was corrected by the Gibbs free energy change in standard state from 1 atm to 1 M (1.89 kcal/mol).

1.1.3. Molecular dynamics (MD) simulations of TACN-guanidine warhead in explicit solvent

The lowest-energy conformer in the preferred diprotonated state of TACN-guanidine warhead obtained in the implicit solvation model was further simulated using classical molecular dynamics in the AMBER force field[10]. The solute molecule was solvated in a 40 Å x 40 Å x 40 Å box of OPC water molecules[11]. The system was neutralized with chloride ions[12]. The atomic charges of the solute were calculated in accord with the RESP procedure[13]. The solute structure was optimized at the HF/6-31G(d) level of theory and the corresponding ESP was generated in Gaussian 09[14]. The RESP charges of the solute were computed using antechamber (AmberTools 22[10]). The bonded terms and van der Waals parameters of the solute were assigned using parmchk2 (AmberTools 22[10]) in accord with the GAFF2 force field.

The system was energy-minimized with the steepest descent method (500 steps) followed by the conjugate gradient method (500 steps) using sander (AmberTools 22[10]). All the subsequent steps were carried out using pmemd.cuda (Amber 2022[10]). The system was thermalized to 298.15 K for 1 ns using Langevin thermostat (with damping constant of 1 ps^{-1}) in the NVT ensemble. The system was equilibrated for 1 ns under pressure of 1 atm isotropically maintained by Monte Carlo barostat. The production run was performed for 100 ns in NPT. In all the simulations, periodic boundary conditions and Particle Mesh Ewald method with a grid spacing of 1.0 Å were used. The bonds involving hydrogens were constrained using the SHAKE algorithm, which allowed to use the integration time step of 2 fs. The cutoff for short-range non-bonded interactions was set to 10 Å. The data were collected every 5 ps.

The hydrogen bonding analysis was carried out using cpptraj (AmberTools 22[10]) to detect solute-solvent interactions. The criteria for hydrogen bonds were donor-acceptor distance of ≤ 3.2 Å and donor-hydrogen-acceptor angle of ≥ 150°.

1.2 Investigating molecular mechanism of DNA cleavage by compound **1**

1.2.1. Building model of DNA complex with ciprofloxacin conjugate

The model of DNA with two fluoroquinolone binding sites was prepared based on the DNA-topoisomerase IV crystal structure (PDB code: 2XKK)[15]. The 26-bp sequence of DNA was extracted and the cleaved sites were resealed. Two models of DNA were prepared, each with one distinct fluoroquinolone binding site. At the binding site, ciprofloxacin conjugated with the aryl linker was aligned to the moxifloxacin molecule, and the latter was removed. The system was neutralized with potassium ions and solvated in a rectangular box with a 15 Å layer of explicit OPC[11] water molecules and 150 mM of KCl[12] in leap (AmberTools 22[10]). The entire system consisted of about 48000 atoms. The OL21 AMBER force field was used for parametrization of DNA[16]. The atomic charges of the ciprofloxacin conjugate were calculated in accord with the RESP procedure[13]. The solute structure was optimized at the HF/6-31G(d) level of theory, and the corresponding ESP was generated in Gaussian 09[14]. The RESP charges of the solute were computed using antechamber (AmberTools 22[10]). The bonded terms and van der Waals parameters of the solute were assigned using parmchk2 (AmberTools 22[10]) in accord with the GAFF2 force field.

1.2.2. Hamiltonian replica-exchange molecular dynamics simulations of DNA complex with ciprofloxacin conjugate

The system was energy-minimized under positional restraints of 100 kcal/mol·Å^2 with the steepest descent method (1000 steps) followed by the conjugate gradient method (1000 steps) using sander (AmberTools 22[10]). All the subsequent steps were carried out using pmemd.cuda (Amber 2022[10]). The system was thermalized for 10 ps (with timestep of 2 fs) using Langevin thermostat (with damping constant of 1 ps^{-1}) from 10.15 K to 100.15 K in the NPT ensemble (Monte Carlo barostat, 1 atm of isotropically controlled pressure). Additionally, 100 ps of dynamics were run to equilibrate the system density. Then, the system was heated for 100 ps using Langevin thermostat from 100.15 K to 298.15 K in the NVT ensemble. Subsequently, the system was equilibrated in NVT by gradually releasing the restraints in 8 steps for 1 ns each. The production run was performed for 100 ns in NPT. Then, the system was subjected to hydrogen mass repartitioning (HMR)[17] in parmed (AmberTools 22[10]) to increase the timestep to 4 fs. The simulation using HMR was continued for 300 ns. In all the simulations, periodic boundary conditions and Particle Mesh Ewald method with a grid spacing of 1.0 Å were used. The bonds involving hydrogens were constrained using the SHAKE algorithm. The cutoff for short-range non-bonded interactions was set to 10 Å. The data were collected every 10 ps.

To enhance the sampling of the ciprofloxacin conjugate at the DNA binding site, we applied Hamiltonian replica-exchange molecular dynamics (H-REMD)[18] implemented in pmemd.cuda.MPI (AmberTools 22[10]). The electrostatic and van der Waals terms of the ciprofloxacin conjugate were scaled. Eight replicas were simulated with the respective scaling factors: 1.0, 0.9, 0.8, 0.7, 0.6, 0.5, 0.4, 0.3. Initially, all the replicas were equilibrated for 10 ns without exchanges. The production run was performed for 2000 ns in NPT with exchanging

attempt every 1000 steps (4 ps). The average acceptance rate of exchange was 0.2, which was sufficient for our study.

The trajectories from the unscaled replica were considered in the analysis using cpptraj (AmberTools 22[10]). To investigate binding mode of the ciprofloxacin conjugate in DNA, the trajectories were aligned to the conjugate and four DNA surrounding nucleobases and averaged. Root-mean-square-deviation (RMSD) of the conjugate coordinates was measured with respect to the system's average structure. At each fluoroquinolone binding site in DNA, we found two clusters representing distinct ciprofloxacin conjugate orientations regarding the DNA nucleobases. From each of the clusters, we extracted 50 representative conformations of DNA by clustering with kmeans algorithm.

*1.2.3. Molecular docking of compound **1** to DNA*

Using the DOCK 6.9 suite of programs[19], compound **1** was docked into the fluoroquinolone binding sites within the DNA conformations obtained by clustering the H-REMD trajectories. The fixed-anchor protocol was used, in which ciprofloxacin position was anchored at the binding site (as in the H-REMD-derived conformations), while the rest of the compound was flexibly docked. The TACN-guanidine warhead was complexed with a single water molecule found in the MD simulations. During docking, the complex with water was kept fixed at the geometry optimized at the B3LYP/6-31G(d) level of theory.

The atomic charges of compound **1** were calculated in accord with the RESP procedure[13]. The structure was optimized at the HF/6-31G(d) level of theory in the extended geometry, and the corresponding ESP was generated in Gaussian 09[14]. The RESP charges of compound **1** were computed using antechamber (AmberTools 22[19]). The atomic charges of water bound by the TACN-guanidine warhead were adopted from the OPC3 water model[20], while the atomic charges of DNA were taken from the OL21 AMBER force field[16].

Subsequently, the box was constructed around the binding site, and electrostatic and steric interactions between a dummy atom and all the DNA atoms were calculated on a 0.2 Å resolution grid within the box by using the grid program. For the energy evaluation, Lennard-Jones potential with 6 for attractive and 12 for repulsive exponents, and Coulomb potential with a distance-dependent dielectric constant of $\varepsilon=4r$ were used.

The docking poses were scored with the grid-based score. The internal energy of the ligand during its growth was described by van der Waals potential with a repulsive exponent of 12. In each step of the growth, a cycle of energy minimization using simplex minimizer was performed with a convergence threshold of 0.1 kcal/mol. Conformers with a score greater than 100.0 kcal/mol were rejected. Finally, one hundred of the best-score conformations were clustered with a 2.0 Å RMSD threshold. To increase the conformational sampling, we repeated the docking 500 times with a different seed in the simplex minimization. The interactions formed between the DNA and compound **1** were analyzed with the cpptraj program (AmberTools 22[10]). To detect the potential nucleophilic attack of the water molecule, bound with the TACN-guanidine warhead of compound

1, at the DNA phosphates, geometric criteria were applied, namely, the O_w-P distance of ≤ 4.0 Å, and the O_w-P-O5' or O_w-P-O3' angles ≥ 150°.

*1.2.4. Building model of DNA complex with compound **1***

The conformations of DNA complex with compound **1** with the highest potential for DNA cleavage identified by docking were further used to build the systems for MD simulations. The system was neutralized with potassium ions and solvated in a rectangular box with a 15 Å layer of explicit OPC[11] water molecules and 150 mM of KCl[12] in leap (AmberTools 22[10]). The entire system included about 52000 atoms. The OL21 AMBER force field was used for parametrization of DNA[16]. The atomic charges of compound **1** were set as in docking. The bonded terms and van der Waals parameters of compound **1** were assigned using parmchk2 (AmberTools 22[10]) in accord with the GAFF2 force field.

*1.2.5. Molecular dynamics simulations of DNA complex with compound **1***

The system was energy-minimized under positional restraints of 100 kcal/mol·Å^2 with the steepest descent method (1000 steps) followed by the conjugate gradient method (1000 steps) using sander (AmberTools 22[10]). All the subsequent steps were performed using pmemd.cuda (Amber 2022[10]). The system was thermalized for 10 ps (with timestep of 2 fs) using Langevin thermostat (with damping constant of 1 ps^{-1}) from 10.15 K to 100.15 K in the NPT ensemble (Monte Carlo barostat, 1 atm of isotropically maintained pressure). Additionally, 100 ps of dynamics were run to equilibrate the system density. Then, the system was heated for 100 ps using Langevin thermostat from 100.15 K to 298.15 K in the NVT ensemble. Subsequently, the system was equilibrated in NVT by gradually releasing the restraints in 8 steps for 1 ns each. The production run was performed for 100 ns in NPT. In all the simulations, periodic boundary conditions and Particle Mesh Ewald method with a grid spacing of 1.0 Å were used. The bonds involving hydrogens were constrained using the SHAKE algorithm. The cutoff for short-range non-bonded interactions was set to 10 Å. The data were collected every 5 ps.

*1.2.6. Refinement of GAFF parameters for compound **1***

The structure of compound **1** was split into two fragments – the ciprofloxacin part with the linker and the TACN-guanidine warhead with the linker. The atomic charges of the fragments were taken from the RESP charges of the complete structure of compound **1** and properly adjusted to obtain integer values of the total charge. The initial bonded and van der Waals terms were assigned in accord with the GAFF force field. Subsequently, the two fragments were reparametrized independently by fitting the parameters such that the AMBER force field energies match those derived from high-accurate quantum chemical calculations[21].

We generated about 5000 conformations of the fragment by applying harmonic restraints imposed on the affected parameters using mdgx (AmberTools 22[10]). The structures were energy-scored in the AMBER force field using pmemd (AmberTools 22[10]) and at the MP2/cc-pVDZ level of theory using PSI4[22]. For the selected angles, force constants and equilibrium values were optimized, while for the dihedral angles only force constants were modified. The latter were

expanded into the Fourier series for up to six terms. The linear least-squares fit between MM and QM energies of the structures was performed using mdgx (AmberTools 22[10]) to produce a set of optimal force field parameters. The procedure was repeated until convergence each time using updated set of parameters.

*1.2.7. Hybrid quantum mechanics-molecular mechanics (QM-MM) dynamics simulations of DNA complex with compound **1***

Three different binding modes of compound **1** in DNA selected from the docking and classical MD were further investigated using QM-MM method implemented in sander (AmberTools24[10]) interfaced with xtb 6.7.0[3] and DFTB+ 24.1[23]. The QM atoms comprised of compound **1** and water molecule bound by the TACN-guanidine warhead, together with two DNA nucleobases that the TACN-guanidine warhead interacted with (about 160-165 atoms in total). The total charge of the QM part was –1. The QM segment was modelled with a set of different semi-empirical methods, such as PM6, AM1, DFTB3 and its variants like DFTB3-D3, DFTB3-D3H4, DFTB3-D42B, DFTB3-D43B, and GFN2-xTB[24,25]. To account for interactions between the QM and MM atoms, electrostatic embedding was applied. The atoms linking the QM and MM regions were treated by the charge-shift scheme. The simulations were carried out in the NVT ensemble. The temperature of 298.15 K was maintained by Langevin thermostat (with damping coefficient of 5 ps^{-1}). The system was equilibrated for 20 ps with the timestep of 0.5 fs. The production run was conducted for 100 ps. The simulations were carried out under periodic boundary conditions. The Particle Mesh Ewald method with a grid spacing of 1.0 Å was used for long-range electrostatics. The bonds with hydrogen in the non-QM part of the system were constrained using the SHAKE algorithm. The cutoff for short-range non-bonded interactions was set to 10 Å. The data were saved every 50 fs.

2. Supplementary tables and figures for computational study

Table S1. Free energies of the lowest-energy conformers of TACN-guanidine warhead in different protonation states calculated at *OpenCOSMO-RS/BP86/def2-TZVP, **OpenCOSMO-RS/BP86/def2-TZVPD, and estimated deprotonation constants. For amines naming, see Figure S5.

Protonated amines	Charge	Free energy* [hartree]	Relative free energy* [kcal/mol]	Free energy** [hartree]	pK_a
-	0	-763.276115	0.00	-763.281998	-
N1	1	**-763.739776**	**0.00**	-763.744207	14.48
N2		-763.726611	8.26		
N3		-763.727545	7.67		
N4		-763.725142	9.18		
N1, N2	2	**-764.197469**	**0.00**	-764.201472	12.20
N1, N3		-764.195488	1.24		
N1, N4		-764.194458	1.89		
N2, N3		-764.180344	10.75		
N2, N4		-	-		
N3, N4		-764.172405	15.73		
N1, N2, N3	3	**-764.640669**	**0.00**	-764.644752	5.77
N1, N2, N4		-764.639931	0.46		
N1, N3, N4		-764.635903	2.99		
N2, N3, N4		-764.614154	16.64		
N1, N2, N3, N4	4	-765.078041	0.00	-765.082755	3.34

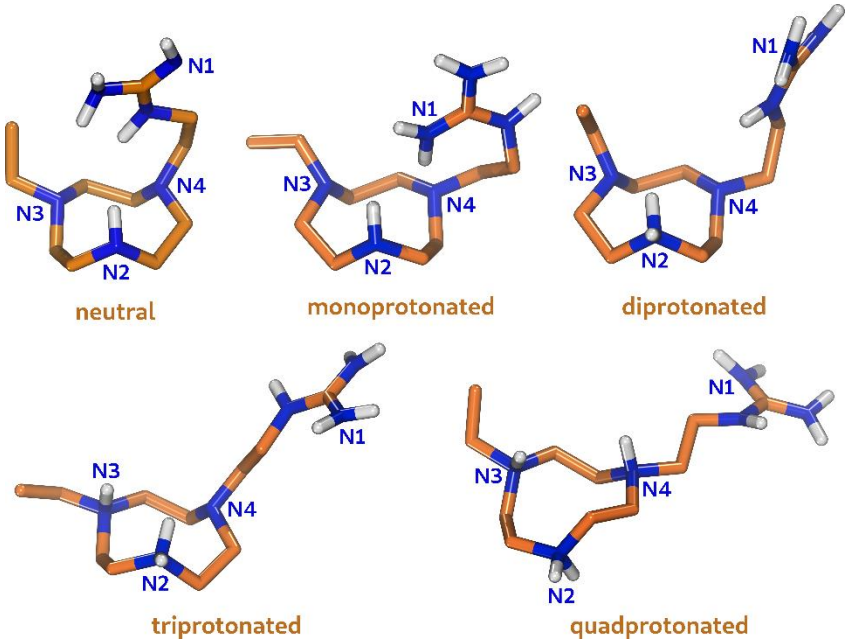

Figure S5. Structures of the lowest-energy conformers of TACN-guanidine warhead in different protonation states.

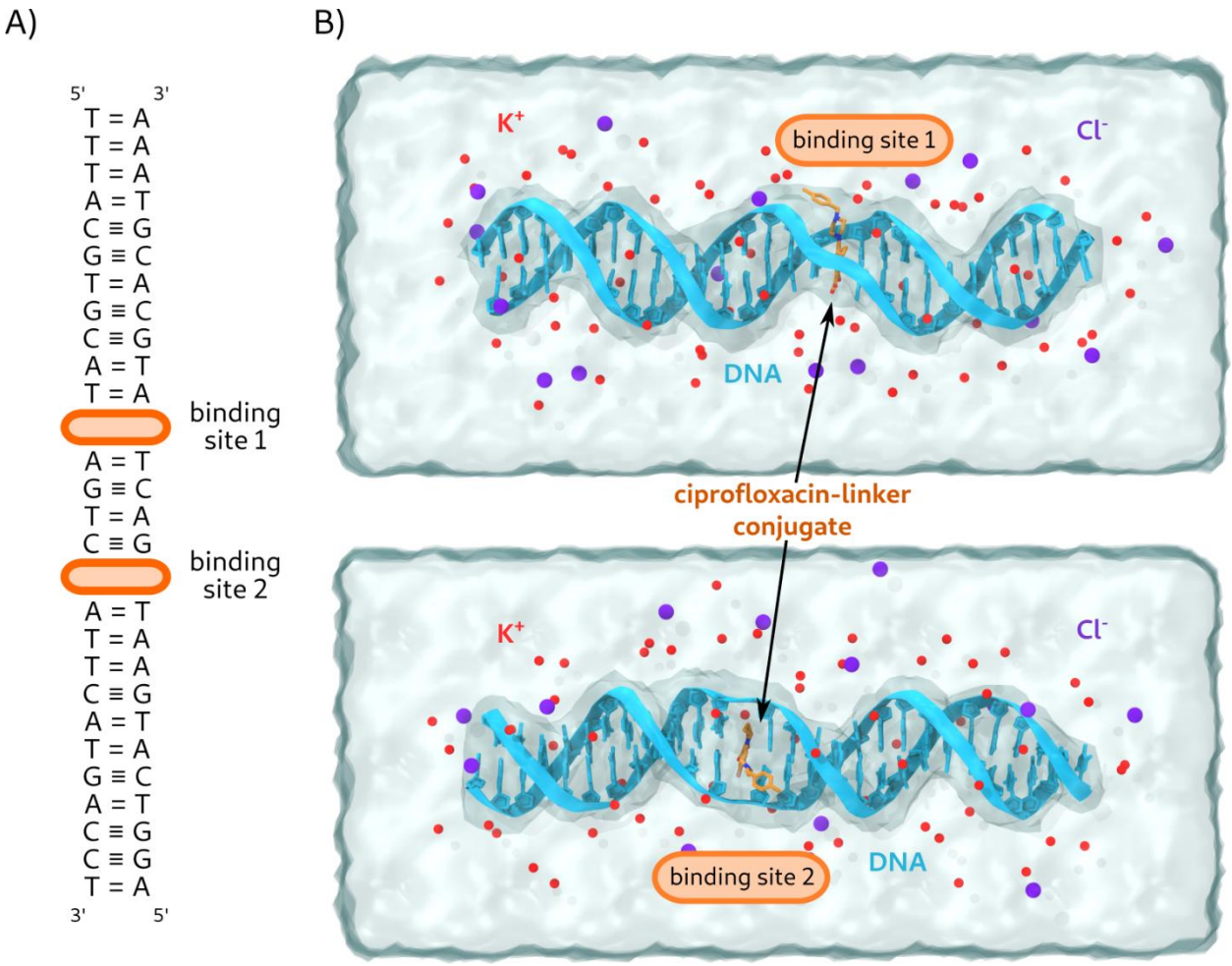

Figure S6. Sequence of DNA adopted from DNA-topoisomerase IV complex (PDB code: 2XKK) and two binding sites occupied by ciprofloxacin-linker conjugate (A). Models of DNA with the ciprofloxacin-linker conjugate bound at two different binding sites (B).

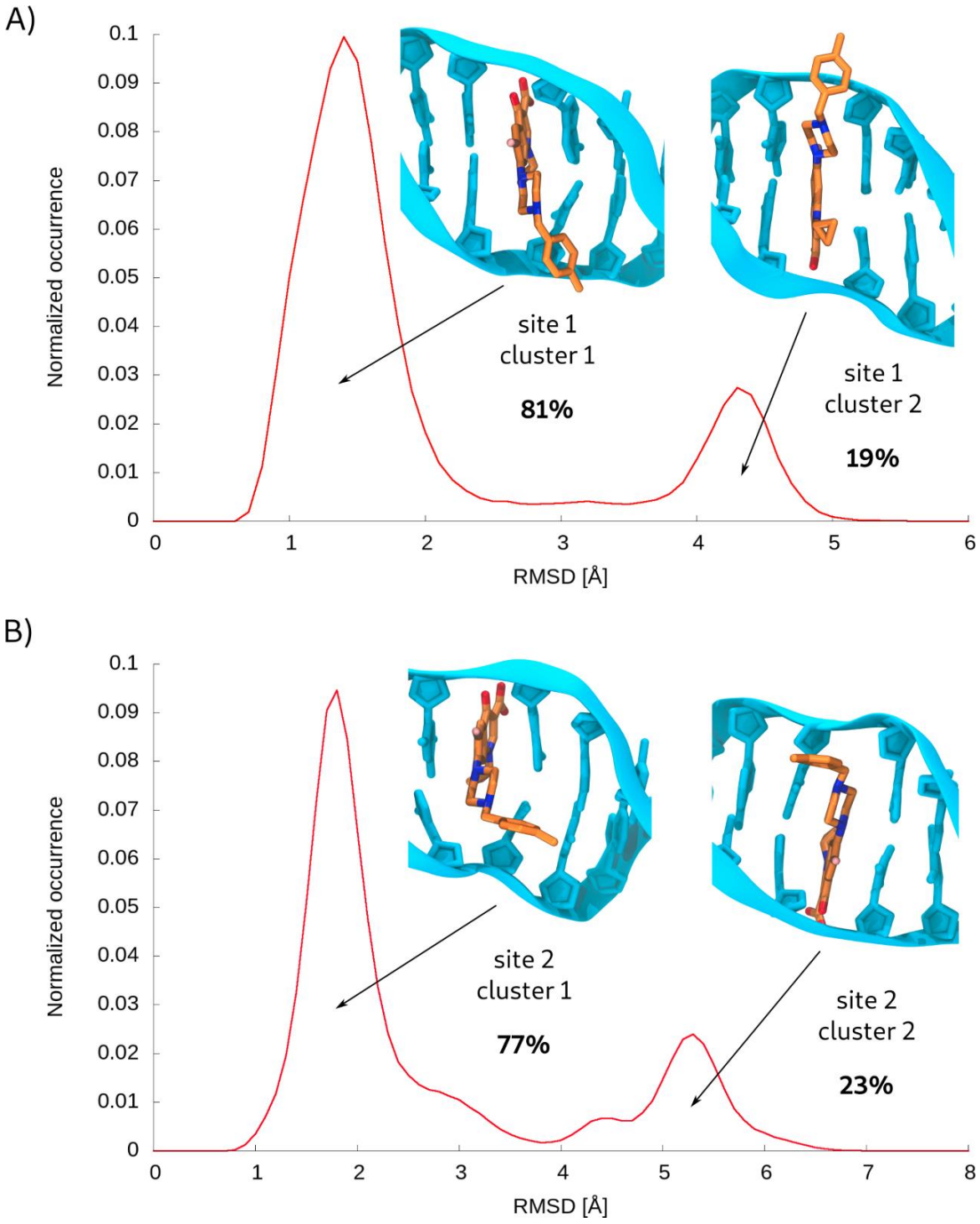

Figure S7. Binding modes of the ciprofloxacin-linker conjugate within the two selected sites in DNA observed in the H-REMD simulations and their populations. At site 1 (A), the orientation of ciprofloxacin perpendicular to DNA bases is preferred (81%) over the parallel orientation (29%). At site 2 (B), only perpendicular orientation of ciprofloxacin is observed with two alternate orientations of the linker.

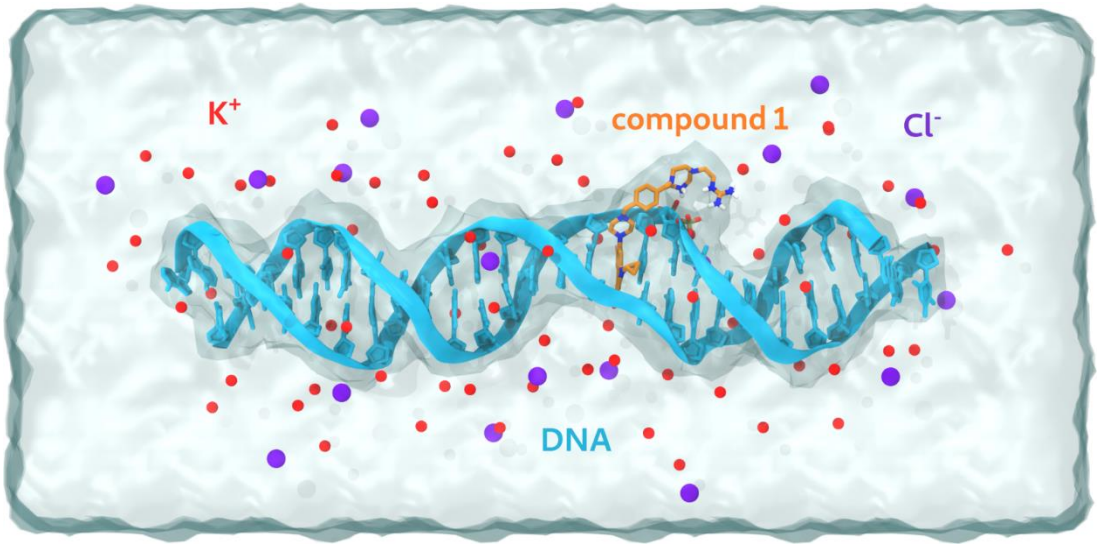

Figure S8. Model of compound **1** bound in parallel orientation of ciprofloxacin at binding site 1 of DNA identified by docking and MD simulations for potential DNA cleavage.

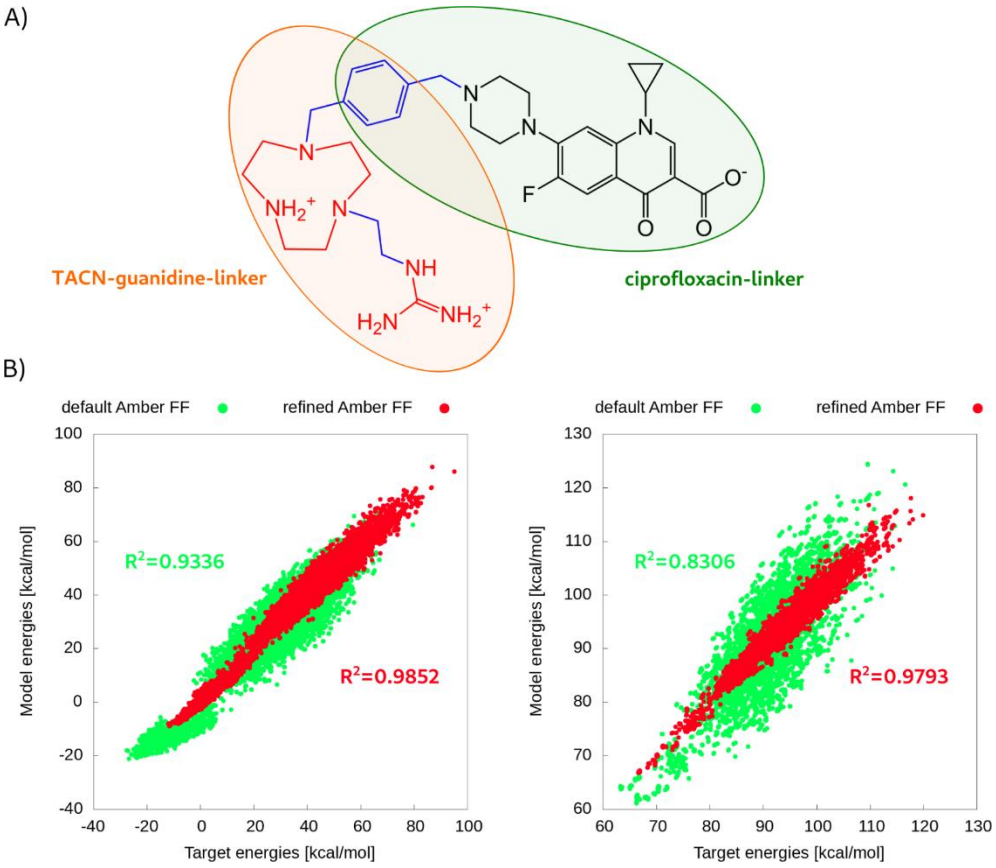

Figure S9. Reparameterization of AMBER force field for compound **1**. Compound **1** split into two separate fragments- ciprofloxacin with linker, and TACN-guanidine warhead with linker (A). Correlation between target energies and model energies of multiple conformations of TACN-guanidine-linker (left) and ciprofloxacin-linker (right) before (green) and after (red) refinement of the AMBER force field parameters (B).

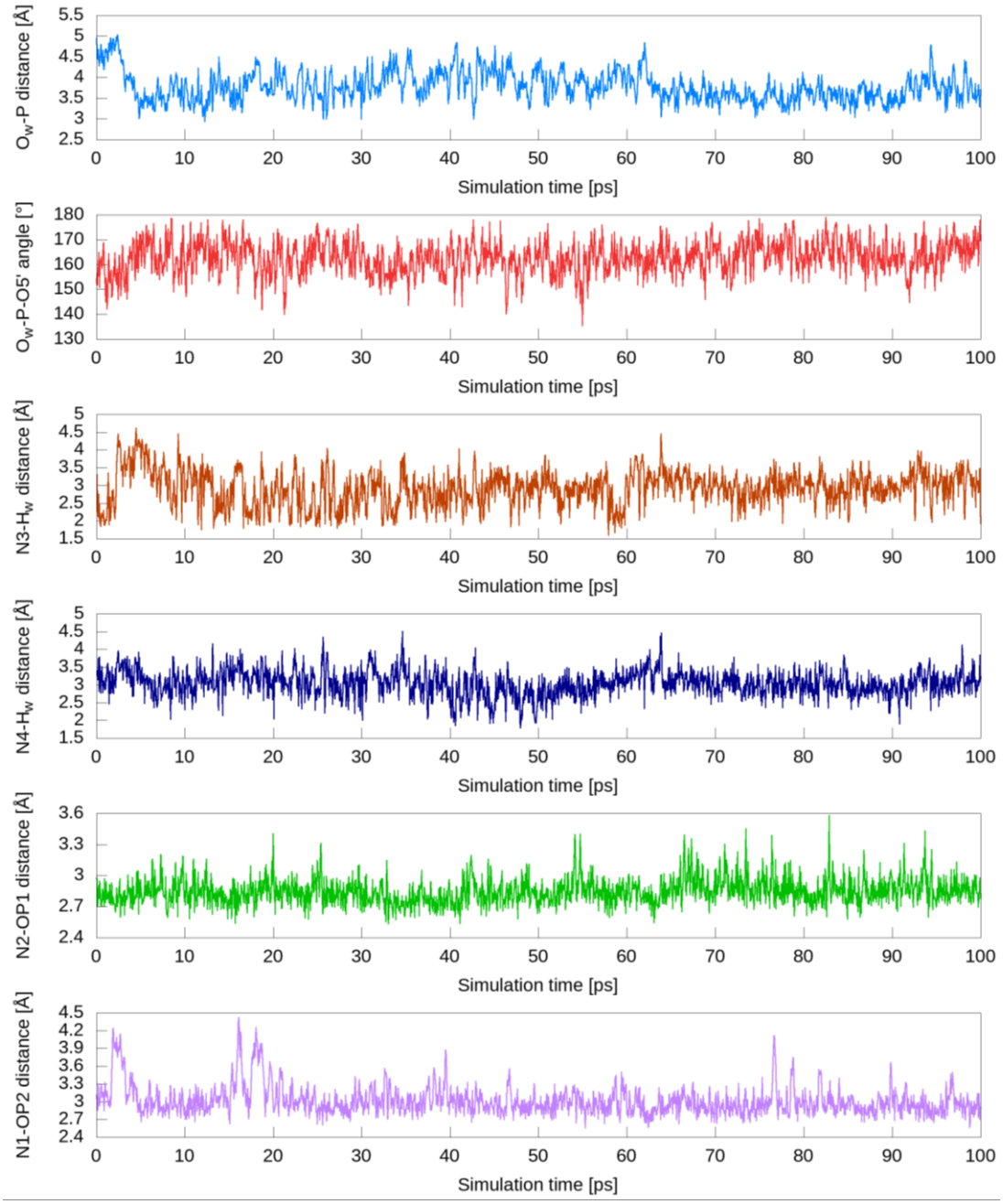

Figure S10. Geometric measures characterizing interactions between DNA and compound **1** in QM-MM simulation, which are essential for DNA cleavage. In-line geometry of the water molecule at the DNA interface is described by the distance between the oxygen atom of water and phosphorus atom of DNA (O_w-P) and the angle between the oxygen atom of water, phosphorus atom of DNA and oxygen atom of the leaving group (O_w-P-O5'). Activation of the water molecule for nucleophilic attack at the DNA phosphate is characterized by the closest distance of any hydrogen atoms of water and tertiary amines of TACN-guanidine warhead (N3-H_w and N4-H_w). Interactions stabilizing the in-line geometry of water are described by two distances – between the secondary amine of TACN and DNA phosphate adjacent to the cleaved phosphodiester (N2-OP1) and between guanidine and cleaved DNA phosphate (N1-OP2).

III. References

1 L. Tjioe, T. Joshi, C. M. Forsyth, B. Moubaraki, K. S. Murray, J. Brugger, B. Graham and L. Spiccia, *Inorg Chem*, 2012, **51**, 939–953.
2 P. Pracht, F. Bohle and S. Grimme, *Phys Chem Chem Phys*, 2020, **22**, 7169–7192.
3 C. Bannwarth, S. Ehlert and S. Grimme, *J Chem Theory Comput*, 2019, **15**, 1652–1671.
4 S. Ehlert, M. Stahn, S. Spicher and S. Grimme, *Journal of Chemical Theory and Computation*, 2021, **17**, 4250–4261.
5 S. Grimme, F. Bohle, A. Hansen, P. Pracht, S. Spicher and M. Stahn, *J Phys Chem A*, 2021, **125**, 4039–4054.
6 F. Neese, *WIREs Computational Molecular Science*, 2022, **12**, e1606.
7 T. Gerlach, S. Müller, A. G. de Castilla and I. Smirnova, *Fluid Phase Equilib*, 2022, **560**, 113472.
8 N. Sadlej-Sosnowska, *Theoretical Chemistry Accounts*, 2007, **118**, 281–293.
9 M. D. Tissandier, K. A. Cowen, W. Y. Feng, E. Gundlach, M. H. Cohen, A. D. Earhart, J. V. Coe and T. R. Tuttle, *The Journal of Physical Chemistry A*, 1998, **102**, 7787–7794.
10 D. A. Case, H. M. Aktulga, K. Belfon, D. S. Cerutti, G. A. Cisneros, V. W. D. Cruzeiro, N. Forouzesh, T. J. Giese, A. W. Götz, H. Gohlke, S. Izadi, K. Kasavajhala, M. C. Kaymak, E. King, T. Kurtzman, T. S. Lee, P. Li, J. Liu, T. Luchko, R. Luo, M. Manathunga, M. R. Machado, H. M. Nguyen, K. A. O'Hearn, A. V. Onufriev, F. Pan, S. Pantano, R. Qi, A. Rahnamoun, A. Risheh, S. Schott-Verdugo, A. Shajan, J. Swails, J. Wang, H. Wei, X. Wu, Y. Wu, S. Zhang, S. Zhao, Q. Zhu, T. E. Cheatham, D. R. Roe, A. Roitberg, C. Simmerling, D. M. York, M. C. Nagan and K. M. Merz, *J Chem Inf Model*, 2023, **63**, 6183–6191.
11 S. Izadi, R. Anandakrishnan and A. V. Onufriev, *J Phys Chem Lett*, 2014, **5**, 3863–3871.
12 A. Sengupta, Z. Li, L. F. Song, P. Li and K. M. Merz, *J Chem Inf Model*, 2021, **61**, 869–880.
13 C. I. Bayly, P. Cieplak, W. D. Cornell and P. A. Kollman, *The Journal of Physical Chemistry*, 1993, **97**, 10269–10280.
14 G. M. J. Frisch, W. Trucks, H. B. ; Schlegel, G. E. ; Scuseria, M. A. ; Robb, J. R. Cheeseman, G. Scalmani, V. ; Barone, B. ; Mennucci, G. A. Petersson, H. Nakatsuji, M. ; Caricato, X. ; Li, H. P. ; Hratchian, A. F. ; Izmaylov, J. ; Bloino, G. ; Zheng, J. L. ; Sonnenberg, M. J. Frisch, G. W. ; Trucks, H. B. ; Schlegel, G. E. ; Scuseria, M. A. ; Robb, G. ; Cheeseman, J. R.; Scalmani, V. ; Barone, B. ; Mennucci, H. ; Petersson, G. A.; Nakatsuji, M. ; Caricato, X. ; Li, H. P. ; Hratchian, A. F. ; Izmaylov, J. ; Bloino, G. ; Zheng, J. L. ; Sonnenberg, K. ; Hada, M.; Ehara, M.; Toyota, R. ; Fukuda, J. ; Hasegawa, M. ; Ishida, T. ; Nakajima, Y. ; Honda, O. ; Kitao, H. ; Nakai, T. ; Vreven, J. E. ; Montgomery, J. A., Jr.; Peralta, F. ; Ogliaro, M. ; Bearpark, J. J. ; Heyd, E. ; Brothers, K. N. ; Kudin, R. ; Staroverov, V. N.; Kobayashi, K. ; Normand, J.; Raghavachari, A. ; Rendell, J. C. ; Burant, S. S. ; Iyengar, J. ; Tomasi, M. ; Cossi, N. ; Rega, J. M. ; Millam, M. ; Klene, J. E. ; Knox, J. B. ; Cross, V. ; Bakken, C. ; Adamo, J. ; Jaramillo, R. ; Gomperts, R. E. ; Stratmann, O. ; Yazyev, A. J. ; Austin, R. ; Cammi, C. ; Pomelli, J. W. ; Ochterski, R. L. ; Martin, K. ; Morokuma, V. G. ; Zakrzewski, G. A. ; Voth, P. ; Salvador, S. ; Dannenberg, J. J.; Dapprich, A. D. ; Daniels, Ö. ; Farkas, J. B. ; Foresman, J. V. ; Ortiz, J. ; Cioslowski and D. J. Fox, *Gaussian, Inc.: Wallingford, CT*.
15 A. Wohlkonig, P. F. Chan, A. P. Fosberry, P. Homes, J. Huang, M. Kranz, V. R. Leydon, T. J. Miles, N. D. Pearson, R. L. Perera, A. J. Shillings, M. N. Gwynn and B. D. Bax, *Nat Struct Mol Biol*, 2010, **17**, 1152–1153.
16 M. Zgarbová, J. Šponer and P. Jurečka, *J Chem Theory Comput*, 2021, **17**, 6292–6301.
17 C. W. Hopkins, S. Le Grand, R. C. Walker and A. E. Roitberg, *Journal of Chemical Theory and Computation*, 2015, **11**, 1864–1874.
18 D. R. Roe, C. Bergonzo and T. E. Cheatham, *J Phys Chem B*, 2014, **118**, 3543–3552.
19 W. J. Allen, T. E. Balius, S. Mukherjee, S. R. Brozell, D. T. Moustakas, P. T. Lang, D. A. Case, I. D. Kuntz and R. C. Rizzo, *J Comput Chem*, 2015, **36**, 1132–1156.
20 S. Izadi and A. V. Onufriev, *J Chem Phys*, 2016, **145**, 074501.
21 R. M. Betz and R. C. Walker, *J Comput Chem*, 2015, **36**, 79–87.

22 R. M. Parrish, L. A. Burns, D. G. A. Smith, A. C. Simmonett, A. E. DePrince, E. G. Hohenstein, U. Bozkaya, A. Y. Sokolov, R. D. Remigio, R. M. Richard, J. F. Gonthier, A. M. James, H. R. McAlexander, A. Kumar, M. Saitow, X. Wang, B. P. Pritchard, P. Verma, H. F. Schaefer, K. Patkowski, R. A. King, E. F. Valeev, F. A. Evangelista, J. M. Turney, T. D. Crawford and C. D. Sherrill, *Journal of Chemical Theory and Computation*, 2017, **13**, 3185–3197.
23 B. Hourahine, B. Aradi, V. Blum, F. Bonafé, A. Buccheri, C. Camacho, C. Cevallos, M. Y. Deshaye, T. Dumitric, A. Dominguez, S. Ehlert, M. Elstner, T. Van Der Heide, J. Hermann, S. Irle, J. J. Kranz, C. Köhler, T. Kowalczyk, T. Kubař, I. S. Lee, V. Lutsker, R. J. Maurer, S. K. Min, I. Mitchell, C. Negre, T. A. Niehaus, A. M. N. Niklasson, A. J. Page, A. Pecchia, G. Penazzi, M. P. Persson, J. Å&tild;ezáč, C. G. Sánchez, M. Sternberg, M. Stöhr, F. Stuckenberg, A. Tkatchenko, V. W. Z. Yu and T. Frauenheim, *J Chem Phys*, 2020, **152**, 124101.
24 Y. Tao, T. J. Giese, Ş. Ekesan, J. Zeng, B. Aradi, B. Hourahine, H. M. Aktulga, A. W. Götz, K. M. Merz Jr. and D. M. York, *J Chem Phys*, 2024, **160**, 224104.
25 E. Caldeweyher, S. Ehlert, A. Hansen, H. Neugebauer, S. Spicher, C. Bannwarth and S. Grimme, *J Chem Phys*, 2019, **150**, 154122.